JBC Papers in Press. Published on December 17, 2015 as Manuscript M115.700385
The latest version is at http://www.jbc.org/cgi/doi/10.1074/jbc.M115.700385

Selective inhibition of the mitochondrial permeability transition pore protects against neuro-degeneration in experimental multiple sclerosis.

Running title: Mitochondrial protection prevents neurodegeneration in MS.

Justin Warne[¥1], Gareth Pryce[¥2], Julia Hill[¥3], Xiao Shi[1], Felicia Lennerås[2], Fabiola Puentes[2], Maarten Kip[1], Laura Hilditch[4], Paul Walker[5], Michela I. Simone[1,5], A.W. Edith Chan[1], Greg J. Towers[4], Alun Coker[7], Michael R Duchen[3], Gyorgy Szabadkai[3,8], David Baker[2]*, David L Selwood[1]*.

[1]The Wolfson Institute for Biomedical Research, University College London, Gower Street, London, WC1E 6BT, UK. [2]Neuroimmunology Unit, Blizard Institute, Barts and the London School of Medicine and Dentistry, Queen Mary University of London, 4 Newark Street, London E1 2AT, UK. [3]Department of Cell and Developmental Biology, University College London, UK. [4]Medical Research Council Centre for Medical Molecular Biology, Division of Infection and Immunity, University College London, UK. [5]Current address: Discipline of Chemistry, School of Environmental and Life Sciences, University of Newcastle, Callaghan, New South Wales, Australia. [6]Cyprotex Discovery Ltd, 100 Barbirolli Square, Manchester M2 3AB, UK. [7]Laboratory of Protein Crystallography, Centre for Amyloidosis and Acute Phase Proteins, UCL Division of Medicine (Royal Free Campus), Rowland Hill Street, London NW3 2PF, England. [8]Department of Biomedical Sciences, University of Padua, Italy.

[¥] Theses authors contributed equally to this paper.
* Joint corresponding authors.

Keywords: cyclophilin D, ppif, permeability transition pore, multiple sclerosis

ABSTRACT

The mitochondrial permeability transition pore (PT pore) is a recognised drug target for neurodegenerative conditions such as multiple sclerosis (MS) and for ischaemia–reperfusion injury in the brain and heart. The peptidylprolyl isomerase, cyclophilin D (CypD, ppif) is a positive regulator of the pore and genetic downregulation or knockout improves outcomes in disease models. Current inhibitors of peptidylprolyl isomerases show no selectivity between the tightly conserved cyclophilin paralogs and exhibit significant off target effects, immune-suppression and toxicity. We therefore designed and synthesised a new mitochondrially-targeted CypD inhibitor, JW47, using a quinolinium cation tethered to cyclosporine (CsA). X-ray analysis was used to validate the design concept and biological evaluation revealed selective cellular inhibition of CypD and the PT pore with reduced cellular toxicity compared to CsA. In an experimental autoimmune encephalomyelitis disease model of neurodegeneration in multiple sclerosis (MS), JW47 demonstrated significant protection of axons and improved motor assessments with minimal immunosuppression. These findings suggest that selective CypD inhibition may represent a viable therapeutic strategy for MS and identify quinolinium as a mitochondrial targeting group for in vivo use.

A considerable body of evidence points to a role for the mitochondrial permeability transition (PT) pore in neurodegenerative and ischaemic cell death. The peptidylprolyl cis-trans isomerase cyclophilin D (CypD, PPIF),which is genomically expressed and imported into mitochondria, is consistently implicated as a key player in the sequence of events leading to PT pore opening and eventual cell death by necrosis. The PT pore forms under conditions of oxidative stress, low adenine nucleotide concentrations and mitochondrial Ca^{2+} overload and results in free

passage of low molecular weight solutes (<1500 Da) and some proteins across the inner mitochondrial membrane. Under these conditions, mitochondrial proton gradient and membrane potential (ψm) is dissipated, leading to ATP hydrolysis by the reversal of the F_1F_O ATP synthase and consequent cellular energy depletion, resulting in cell death. Recent studies point to the F_1F_O ATP synthase of mitochondria as being the major component of the PT pore (1), but the subunits involved and the exact pore forming mechanism is controversial (2-4). CypD binds to the lateral stalk of the F_1F_O ATPase and positively regulates pore opening (5,6). In CypD knockout animals, the pore is desensitized to Ca^{2+}, in an inorganic phosphate(P_i)-dependent manner (7). There is mounting evidence that CypD is key in mediating Ca^{2+} induced pore opening, and its absence e.g. in PPIF knockout animals, desensitizes the pore to Ca^{2+}, in an inorganic phosphate(P_i)-dependent manner (7). Pharmacological inhibition of the pore offers a route to cyto- and neuroprotection.

Multiple sclerosis (MS) is an immune-mediated demyelinating and neurodegenerative disease of the central nervous system and the commonest form of non-traumatic disability in young adults (8). Whilst relapsing autoimmunity in MS can be controlled by peripheral immunomodulatory agents, progressive disability that results from neurodegeneration is so far, untreatable(8,9). Neurodegeneration in MS is associated with the influence of centrally-active inflammatory responses(10,11). This may relate to metabolic and energy stresses in nerves within the inflammatory penumbra that drive nerve loss during neuroinflammation in MS and other neurodegenerative diseases(12-14). Mitochondrial dysfunction and the irreversible opening of the PTP, is now recognised as a key player in the degeneration of axons (15). In MS lesions (12,16,17),the PT pore induced ATP deficit may result in the inactivation of energy-dependent sodium/potassium pumps, leading to sodium loading and the reversal of the sodium-calcium exchanger that causes toxic accumulation of calcium ions and the induction of cell death effector pathways(16,18).

CypD is highly expressed in a subset of astrocytes , microglia and neurons (19) where it may contribute to excitotoxicity and cell death in MS lesions (12,16,17). CypD knockout mice show a less severe phenotype compared to wild type in the experimental autoimmune encephalomyelitis (EAE) model of MS(20,21). CypD knockout mouse studies in models of traumatic brain injury (22,23), Alzheimer's disease (24,25), Parkinson's disease (26), amyloid lateral sclerosis (27) and Huntington's disease (28,29), all show a benefit compared to wild type mice. The PT pore is also implicated in ischaemia–reperfusion injury in the adult brain (30)and in the heart where CypD ablation, or RNAi knockdown (31,32) provide cardio-protection(33,34). A selective inhibitor of PT pore opening could therefore have therapeutic applicability in a range of diseases particularly MS where the progressive disability that results from neurodegeneration is so far, untreatable(8,9).

Cyclosporine (cyclosporin A, CsA, Fig. 1*A*) is a non-selective cyclophilin inhibitor. CsA forms a ternary complex with the cytoplasmic CypA and calcineurin leading to inhibition of calcineurin signaling. This blocks downstream cytokine production associated with immune cell activation(35) (36) and makes CsA a potent and clinically useful, immuno-suppressive. Chemical modification to remove calcineurin binding is relatively straightforward, but selectivity for the different cyclophilin proteins is difficult owing to their close structural and sequence similarity(37). Neuroprotective actions of CsA via action on mitochondrial CypD are reported: case studies and clinical trials support a neuroprotective effect (38,39), while clinical studies with CsA in traumatic brain injury are in progress (NCT01825044). *In vitro* CsA shows cytotoxicity and multiple effects on cell health parameters, while problems with the clinical use of CsA are nephrotoxicity(35,39), bilirubinaemia and liver toxicity(40) which can require withdrawal of the drug. These properties combine to make CsA a less than ideal drug candidate for neuroprotection.

A potential solution to the problem of targeting the individual cyclophilins is to enable mitochondrial localization. Triphenylphosphonium (TPP^+) is the archetypal mitochondrial targeting, lipophilic cation(41) and has been used in humans for targeting a co-enzyme Q analogue to mitochondria(42). TPP^+ has non-ideal pharmaceutical properties however, including: a) high molecular weight and lipophilicity contributing to a lack of "drug likeness", b)

mitochondrial toxicity (43,44), d) effects on respiration(45) and c) non-ideal biodistribution (46). We have previously shown that TPP^+ can be linked to CsA at the $[Sar]^3$ position to provide a molecule with immunosuppression blocked and improved cytoprotection in vitro (36,47).

Here we investigated the quinolinium cation as a replacement for triphenylphosphonium. We observed that quinolinium is an effective mitochondrial targeting group: A prototype molecule JW47, was shown to be more potent at blocking the PT pore and demonstrated less cell toxicity than CsA. In vivo JW47 was less immunosuppressive than CsA and notably achieved significant neuroprotection in an EAE model of MS in mice.

Experimental procedures

Chemistry. All commercially available solvents and reagents were used without further treatment as received unless otherwise noted. NMR spectra were measured with a Bruker DRX 500 or 600 MHz spectrometer; chemical shifts are expressed in ppm relative to TMS as an internal standard and coupling constants (J) in Hz. LC-MS spectra were obtained using a Waters ZQ2000 single quadrupole mass spectrometer with electrospray ionisation (ESI), using an analytical C4 column (Phenomenex Gemini, 50 x 3.6 mm, 5 μm) and an AB gradient of 50–95 % for B at a flow rate of 1 mL/minute, where eluent A was 0.1:5:95 formic acid/methanol/water and eluent B was 0.:5:95 formic acid/water/methanol. High resolution mass spectra were acquired on a Waters LCT time of flight mass spectrometer with electrospray ionisation (ESI) or chemical ionization (CI).

Preparation of JW47, 1-(pent-4-enyl)quinolinium To a solution of quinoline (1 g, 7.74 mmol) in EtOAc was added 5-bromo-pent-1-ene (1.27 g, 8.51 mmol) and this mixture was heated to reflux overnight. The mixture was allowed to cool before concentration under reduced pressure. The product was isolated as a light brown oil (1.54 g, 99%).

LCMS (*m/z*): $[MH]^+$ calcd. for $C_{14}H_{16}N+$, 198.29; found 198.10. NMR δ_H (Acetone-d6, 600 MHz): δ 10.26 (dd, *J* = 5.8, 1.4 Hz, 1H), 9.41 (d, , *J* = 8.4 Hz, 1H), 8.80 (d, *J* = 9.0 Hz, 1H), 8.58 (dd, *J* = 8.2, 1.3 Hz, 1H), 8.36 (dd, *J* = 8.3, 1.5 Hz, 1H), 8.27 (dd, *J* = 8.3, 5.8 Hz, 1H), 8.13 – 8.08 (m, 1H), 5.90 (dd, *J* = 17.0, 10.3 Hz, 1H), 5.49 – 5.42 (m, 2H), 5.09 (ddd, *J* = 17.1, 3.4, 1.6 Hz, 1H), 1H), 5.01 – 4.96 (m, 1H), 2.41 – 2.35 (m, 2H), 2.34 – 2.26 (m, 2H).

[Gly-(1S,2R,E)-8-quinolinium-1-hydroxy-2-methyloct-4-ene][1] *CsA (JW47)* To a solution of Cyclosporin A (75 mg, 0.06 mmol) in DCM (2 mL) was added 1-(pent-4-en-1-yl)quinolinium (23 mg, 0.072 mmol) and Hoveyda-Grubbs 2nd generation catalyst (7 mg, 0.01 mmol, 17mol%). The reaction was stirred in the microwave at 90 °C for 30 minutes and then allowed to cool. Triethylamine was added to the mixture and then stirred overnight with excess $P(CH_2OH)_3$ to coordinate the ruthenium catalyst. This was then washed away with brine and water before the mixture was passed through a Stratospheres PL Thiol MP SPE cartridge (polymer Lab, Varian Inc) to remove any remaining catalyst. The crude product was purified by flash reverse-phase chromatography (MeOH:H_2O:formic acid) to give JW47 as a brown solid (15 mg, 17%). HRMS (*m/z*): $[MH]^+$ calcd. for $C_{65}H_{115}N_{11}O_{12}$, 1357.92; found 1357.95. NMR δ_H ($CDCl_3$, 600 MHz): δ 3.49 (s, NMe, 3H), 3.40 (s, NMe, 3H), 3.20 (s, NMe, 3H), 3.12 (s, NMe, 3H), 3.08 (s, NMe, 3H), 2.71 (s, NMe, 3H), 2.68 (s, NMe, 3H).

NMR δ_C ($CDCl_3$, 150 MHz): 39.35, 39.19, 33.67, 31.25, 30.10, 30.01, 29.79 (7 x N-Me).

Protein expression. The CypD expression system was constructed as described by Schlatter et al (48). Briefly, codon optimised DNA encoding the CypD-K133I gene was cloned into pET11a (Novogen) digested with NdeI and BamHI. The resulting plasmid was used to transform BL21(DE3)pLysS. Expression cultures were grown at 37°C in Luria–Bertani (LB) medium, at A_{600} of 0.6, the cells were induced with 1 mM isopropyl-d-1-thiogalactopyranoside (IPTG). The cultures were then incubated at the same temperature for another four hours and the cells harvested by centrifugation. The cell pellet was re suspended in lysis buffer (100mM Tris/HCl pH 7.8, 2mM EDTA, 2mM DTT supplemented with EDTA-free protease inhibitor tablets (Roche)) and the cells lysed by sonication. The sonicate was clarified by centrifugation and the CypD was isolated as previously described (49) using IEC with SP-Sepharose followed by Q-sepherose and finally SEC with Superdex200. The protein was

stored in SEC buffer (50mM potassium/sodium phosphate pH 7.3, 100mM NaCl, 2mM EDTA, 0.02% sodium azide) at 4°C.

*Crystallography***.** Crystals were grown using the hanging drop method as previously described (50); drops contained a 50:50 mix of protein solution (30 mg/ml CypD in gel filtration buffer) and reservoir solution. The best crystals were obtained with a reservoir solution consisting of 23% polyethylene glycol (PEG3350), 50 mM sodium-citrate buffer at pH 2.9 as precipitant solution. Prior to data collection the crystals were cooled to 100K using 35% PEG 3350 in sodium-citrate buffer at pH 2.9 as the cryoprotectant. Data were collected on beam-line i04 at Diamond Light Source. Phases were determined by the molecular replacement method using the PHASER (51) from the CCP4 suite of programmes (52); the CypD-cyclosporin A structure, pdb code 2z6w, was used as the search model, but with the cyclosporin A removed from the model. The model was refined using cycles of the programme REFMAC (53) (54) (with aniosotropic B-factors and Babinet bulk solvent modelling), interspersed with manual checks and model building with COOT (55). The final resolution cut-off was determined during refinement. Ligand topologies were generated with PRODRG2 (56). The final model was validated with PROCHECK (57) and SFCHECK (54) and finally MOLPROBITY (58). Refinement statistics are presented in Table 1. The illustrations were produced with the PyMOL molecular graphics system (Shrödinger LLC).

Fluorescence Polarization assay. Fluorescence polarization (FP) is inversely related to the molecular rotation of the fluorophore. Fluorophores linked to small molecules tumble faster and emit less polarized fluorescence than fluorophore-small molecules bound to proteins. FP is a convenient technique to measure affinity of ligands to cyclophilins (59,60). We synthesized a new fluorescein-PEG-CsA ligand as the probe (vide supra) and we determined the binding of our novel ligands to CypD and CypA.

Titration of a single probe concentration against different enzyme concentrations was used to determine the dissociation constant (Kd). From this we also determined the enzyme concentration that would give a high enough polarization signal to measure binding affinities. The inhibitor constants (Ki), were calculated with the equation below (61).

$$Ki = \frac{[I]50}{\frac{[L]50}{Kd} + \frac{[P]0}{Kd} + 1}$$

Where [I]50 is the concentration of the unlabelled compound at 50% inhibition, [L]50 is the concentration of the free probe-cyclophilin enzyme at 50% inhibition, [P]0 is the concentration of the free protein at 0% inhibition, and Kd is the dissociation constant of the probe-protein complex

Assays were conducted in 384-black low flange non-binding microtiter plates (Corning, Tewksbury, MA, USA). A total solution of 80 µL was used consisting of 3 components, fluorescent cyclosporine probe (FP-CsA) 45 nM, enzyme 40 nM, inhibitor (10-10000 nM). At least 3 replicates were used for each experiment. DMSO% in total solution should remain lower than 1%. FP-probe. Enzyme, inhibitor and FP-CsA are incubated in the OmegaFluostar at room temperature for 30 minutes, FP-CsA (40 µL) was added last. Measurements were taken after gain adjustment of control sample and 30 min incubation, with a xenon flash light with filter settings for 485 excitation and 520 emission.

Mitochondrial isolation. Subcellular fractionation was performed as previously described (62). Briefly, C57BL/6J WT or cypD(63) -/- male mice of 3-6 months were sacrificed by cervical dislocation, and their liver was removed and placed immediately into ice-cold isolation buffer (250mM mannitol, 5 mM HEPES, 0.5 mM EGTA, pH 7.4). At 4°C, the liver was rinsed in PBS to remove excess blood, and any fat and connective tissue was eliminated. PBS was then replaced with isolation buffer containing 1 mM PMSF, and the liver was chopped into pieces (approximately 2 mm in length). Tissue was then homogenized in this solution until no solid matter remained, and then centrifuged at 800g for 10 minutes at 4°C. The nuclear pellet was then discarded, and the post nuclear supernatant retained, and centrifuged at 10300G for another 10 minutes at 4°C. The post-mitochondrial supernatant was discarded, and the mitochondrial pellet was resuspended in isolation buffer and PMSF, and kept on ice. Protein levels were quantified using a ThermoScientific BCA protein

quantification assay, as per manufacturer's instructions.

Calcium retention capacity assay. Isolated mitochondria were resuspended (500 µg protein/ml) in MSK buffer (75 mM mannitol, 25 mM sucrose, 5 mM potassium phosphate monobasic, 20 mM Tris-HCl, 100 mM KCl, and 0.1% bovine serum albumin, pH 7.4) supplemented with 10 mM succinate, 1 µM rotenone and 1 µM Fluo5N. 200 µl mitochondrial suspension per well was used in 96 well microplates. Compounds were incubated for ten minutes before the plate was assayed in a Fluostar Optima plate reader, using Ex/Em filters at 480/520 nM; $CaCl_2$ was injected approximately every 6.5 minutes for 80 minutes (12 total injections, final concentration of 75 µM). To calculate % inhibition of Ca^{2+} induced pore opening, first areas under each curve were calculated, and controls without $CaCl_2$ addition were subtracted as background. The background corrected values were then expressed as the fraction of controls without mitochondria, representing the total amount of Ca^{2+} added, unbuffered by mitochondria. Percentage inhibition for each [compound] was then calculated as the % of the corresponding value for the untreated condition. Significance was assessed by one way ANOVA, in comparison to CsA control. For experiments with CypD -/- mice, 100ul mitochondrial suspension per well was used. $CaCl_2$ was injected approximately every 6.5 minutes for 135 minutes (20 total injections, final concentration of 266 µM). Data were background corrected and expressed as the fraction of controls without mitochondria, and then normalised to the wild type no drug condition. Significance was assessed by one way ANOVA.

*Respirometry***.** Oxygen consumption was measured using Oroboros Oxygraph-2K as previously described (62). Prior to the assay, the Oxygraph chambers were calibrated with Miro5 buffer (0.5 mM EGTA, 3 mM $MgCl_2.6H_2O$, 60 mM K-lactobionate, 20 mM taurine, 10 mM KH_2PO_4, 20 mM HEPES, 110 mM sucrose, 1 g/l BSA (essentially fatty acid free)). Isolated mitochondria were suspended in Miro5 (at 100-200 µg/ml), loaded into the chamber together with substrates (malate, 2 mM; glutamate, 10 mM), and the O_2 flow signal was allowed to stabilise to the basal respiration rate (approx. 10 min). Compounds were added to the chambers at the following concentrations and order: DMSO/CsA/JW47 (concentration as indicated) to produce basal rate after compound (basal AC), ADP (2.5 mM) to give state 3 respiration, oligomycin (2.5 µ M) to give leak respiration, FCCP (titrated to produce maximal respiratory capacity), and antimycin A (2.5 µM) to give non-mitochondrial respiration. Data were analysed by subtracting the antimycin A respiration rate to give mitochondrial specific O_2 flow, and were then expressed as a percentage of the basal O_2 flow. Significance was assessed by one way ANOVA, in comparison to DMSO control.

Measurement of mitochondrial membrane potential. Rat cortical neurons, cultured for 8-9days, were incubated for 40 minutes at 37°C with the cell permeant cationic dye tetramethylrhodamine methyl ester (TMRM, 25 nM), and fluorescence was measured using the ImageXpress Micro XL system (Molecular Devices). Fluorescence was measured for 7 minutes prior to addition of DMSO, CsA or JW47 (both at 40 nM and 1 µM), and then for a further 50 minutes before the addition of the mitochondrial uncoupler carbonyl cyanide-*4*-(trifluoromethoxy)phenylhydrazone (FCCP, 5 µM) as a positive control. The minimum value after the addition of compound (prior to the addition of FCCP) was taken, and this was expressed as a % (using baseline as 100% and FCCP as 0%), and then normalized to DMSO (100%). Significance was assessed by one-way ANOVA, in comparison to DMSO control.

Measurement of mitochondrial membrane potential (ex vivo). Freshly isolated mouse liver mitochondria were suspended in MSK buffer containing 10ug/ml rhodamine123 (dequench mode), at a concentration of 500ug/ml, and plated in an opaque black 96 well plate. Baseline fluorescence was then measured every 60 seconds for 5 minutes in a Fluostar Optima (Ex480/Em520) before manual addition of compounds (concentrations as specified). Fluorescence measurements were continued for 45 minutes until the addition of 2uM FCCP, followed by a further 10 minutes of fluorescence readings.

ATP production. Freshly isolated mitochondria were resuspended in MSK buffer (containing10mM glutamate and 2mM malate) at

1mg/ml and plated in opaque white 96 well plates, or for neuronal assays, neurons were used 9 days after plating at 15000 cells/well. Drugs were added at the concentrations specified, and for mitochondrial assays were incubated for ten minutes before addition of ADP (5mM), followed by another 45 minutes. For neuronal assays, drugs were added in neurobasal medium and incubated for 60 minutes. Cell Titer Glo reagent was then added, and the plate shaken for 2 minutes in the dark to lyse cells/mitochondria and release ATP. The plates were incubated a further ten minutes and then luminescence values read using an Optima FluoStar. ATP production: Data were normalised to DMSO control, and significance assessed by one way ANOVA. Brain mitochondria are insensitive in this assay.

Cytotoxicity in HepG2 cells. HepG2 cells were seeded in black, clear-bottom 96-well tissue culture plates at a density of 3000 cells per well. The cells were incubated for 24 h in culture medium and then exposed (in three replicates) to increasing doses of test compound or to vehicle control (0.5% DMSO). The cells were exposed for 72h before running the high content screening (HCS) assays. The HCS assay was multiplexed to determine mitochondrial membrane potential and mitochondrial mass using MitoTracker® (Life Technologies), cytochrome C release (antibody, Abcam), membrane permeability, YO-PRO^{TM}-1 (Life Technologies). Cell count, nuclear size and DNA structure were also measured Hoechst 33342 (Life Technologies). Following staining of the HepG2 cells fluorescence was analyzed by image acquisition with a Thermo Fisher Cellomics® ArrayScanVTI High Content Screening Reader (ThermoFisher Scientific Inc., Waltham, MA) and vHCS^{TM}view software (ThermoFisher Scientific Inc.). Twenty fields were imaged per well using a 10x wide field objective. The image acquisition data were normalized to vehicle control values. Dose-response curves were defined and evaluated with the following equations:

(1) $\xi(C; c; \omega) \equiv (\ln(C) - c)/\omega;$
(2) $t(\xi) \equiv (1 + \tanh(\xi))/2;$
(3) $R(t;R0;R\infty) \equiv R0(1 - t) + R\infty t;$

In which C represents the test compound concentration and R0, R∞, c, and ω are fitting parameters. The final response at a given concentration C is expressed as $R(t(\xi(C; c; \omega));R0;R\infty)$. It was restricted such that $\omega > 0$, which implies $R \rightarrow R0$ as $C \rightarrow 0$ and $R \rightarrow R\infty$ as $C \rightarrow \infty$. The coefficient of determination (R^2) was calculated for each compound and dose-response curve. An R^2 value of greater than 0.65 was used as QC criteria and was required in all response curves.

Cell based assay for CypA activity. VSV-G pseudotyped GFP-encoding HIV-1 vector was prepared by triple plasmid transfection of 293T cells with Fugene 6 (Roche) as follows. Confluent 293T cells in a 10cm dish were transfected with a mixture of 10 µl Fugene-6 in 200µl OptiMEM (Gibco), with 1 µg of pMDG VSV-G expression vector (64), 1 µg of p8.91 HIV-1 gag-pol expression vector (65), and 1.5 µg of lentiviral expression vector encoding enhanced GFP protein, CSGW (66). Viral supernatant was collected 48h post transfection and stored at -80^{o}C.

To generate CRFK cells stably expressing N-terminally HA-tagged TRIM-CypA from an EXN-based vector, MLV vector was prepared as above, using pMDG, CMVi MLV gag-pol expression vector, and gammaretroviral expression vector encoding a fusion protein comprising human CypA downstream of owl monkey TRIM5 RBCC (EXN-TRIM-CypA) (67). CRFK cells, which are null for TRIM5α activity (68) were then transduced with vector, followed by selection of cells in 1 mg/ml G418 (Invitrogen).

To test for the ability of drug to rescue HIV-1 infectivity in the presence of TRIM-CypA, CRFK cells were infected with a single dose of virus that infected around 20% of the cells, in the presence of DMSO, CsA (0.3-10 µM) or JW47 (0.6-20 µM). Infectivity was measured by flow cytometry, 48 hrs post infection.

Pgp activity. Assessment of drug transporter activity was made using the Pgp-GloTM assay (Promega, Madison, WI, USA) containing recombinant human ABCB1 in membranes and according to the manufacturer's instructions. Briefly, samples were pre-incubated with ATP before incubation with 100 mM compound or positive control. The residual ATP was assayed by luciferin bioluminescence.

In vitro mitogenic T cell stimulation. Spleens were isolated from ABH mice and tissue was homogenized through a cell strainer (BD Biosciences, Oxford, UK) into Dulbecco's

modified eagle medium (DMEM; Invitrogen, Paisley, UK) containing 10 % foetal calf serum (FCS, Gibco, Invitrogen), 2 mM L-glutamine (Invitrogen, UK), 100 U/ml penicillin and 100 µg/ml streptomycin (Invitrogen) and 50 µM 2-mercaptoethanol (Invitrogen). Cells were centrifuged at 500g for 5min and erythrocytes were lysed using 0.87 % ammonium chloride following incubation for 5 min at 37˚C. Cells were washed and viable cells counted using trypan blue (Sigma Aldrich, Poole, UK) exclusion. 4 x 10^{-5} cells/well were incubated 96 well microtest U-bottom plates (Falcon BD, Oxford UK) in final volume of 200µl DMEM medium. Cells were incubated with either ten-fold dilutions (range 10nM-10µM) of CSA (Sandoz, Basel, CH) or JW47 diluted in DMEM medium from a 50mM stock in dimethyl sulphoxide. Cells were incubated with either: 5µg/ml concanavalin A (Con A. Sigma Aldrich) mitogen; 0.5µg/ml mitogenic mouse CD3 and mouse CD28-specific antibodies (Pharmingen, Oxford, UK). The cells were incubated in 37˚C during 18-22 h, before addition of 1 µCi ^{3}H-thymidine (PerkinElmer, MA, USA) per well. After additional incubation in 16-20 h the 96-well plates (Microtest U-bottom, Falcon BD) were harvested (Harvester 96, Mach III M, TOMTEC) onto glass-fibre filters (PerkinElmer). After drying, a scintillation sheet (MeltiLexA; PerkinElmer) was melted onto the filter using a hot plate (RET Basic, IKA, Germany). Samples were analysed using scintillation counting (MicroBeta Plus, Liquid Scintillation Counter, PerkinElmer, WallacOy, Finland) and ^{3}H-thymidine incorporation was assessed in at least triplicate samples.

*Myelin antigen-induced T cell proliferation***.** ABH mice were injected subcutaneously in the flank with 100 µg myelin oligodendrocyte glycoprotein (MOG) peptide residues 35-55 (Cambridge Research Biochemicals Ltd, Billingham, UK) emulsified in Freunds adjuvant containing 200 µg *Mycobacterium tuberculosis* H37Ra (DifcoBacto, MI, USA) on day 0 and 7 (69). Spleens were collected and prepared and analysed as above except that mitogens were replaced with 5µg/ml MOG 35-55 peptide and cells were incubated for 72h before addition of tritiated thymidine.

Pharmacokinetic analysis. ABH mice (n=4) were injected intraperitoneally with 0.1 ml of either 10 mg/kg JW47. Animals were killed 2h and 4h later with $C0_2$ overdose and blood was immediately collected from the heart following death and added to Microtainer (BD, Oxford, UK) tubes, centrifuged using an Eppindorf microfuge and plasma collected. Following the remove of blood the brain was rapidly (<30s) dissected from the skull and stored at -80°C prior to analysis by a Contract research Organisation (CRO) using liquid crystal mass spectroscopy.

*In vivo T cell proliferation.*The contact sensitiser 4-ethoxymethylene-2-phenyl-2-oxazolin-5-one (oxazolone, OX, Sigma) was dissolved (25 mg/ml) in 4:1 acetone:olive oil (AOO). Mice (n=3 per group) received epicutaneous application of either 25 µl of 2.5% OX or AOO on the dorsum of the ear on day 0 (70). The draining auricular lymph nodes were removed three days later and the induced proliferative response was assessed as previously described. Briefly, 5 x 10^{5} cells per well were cultured in RPMI-1640 medium with glutamate (Gibco®, Invitrogen Ltd, Paisley UK), supplemented with 0.5mM sodium, in round-bottomed 96 well plates overnight at 37°C in a humidified atmosphere of 5% CO_2.In the presence of 1 µCi ^{3}H-thymidine (PerkinElmer, MA, USA) per well. DNA synthesis was estimated using beta scintillation counting as above Animals received daily i.p. injections of either vehicle or JW47 from day zero to three (14,70). Results are expressed as mean± SEM thymidine incorporation counts per minute (CPM)

Induction of relapsing-progressive EAE. Mice were injected subcutaneously (s.c.) with 1mg freeze-dried mouse spinal cord homogenate (SCH) in Freunds adjuvant on day zero and seven as described previously (71). After the initial paralytic disease and subsequent remission, a relapse was induced by a further injection of SCH in Freunds incomplete adjuvant on day 28 to induce a relapse 7 days later (71). Studies were randomised, blinded and powered as described previously (71). Neurological scores were graded as 0 = normal; 1 = limp tail, 2 = impaired righting reflex, 3 = hindlimb paresis, 4 = complete hindlimb paralysis, and 5 = moribund/death (71). Results are expressed as mean ± SEM maximum or minimum neurological score and mean day of onset± SD. The clinical scores are presented as the mean daily neurological score ± standard error of

the mean (SEM). Differences in clinical scores were assessed using non-parametric, Mann Whitney U statistics(71). Motor control and co-ordination was assessed on an accelerating (4 – 40 rpm, accelerating at 6rpm/25s) RotaRod (ENV-575M, Med Associates Inc, St. Albans, VT, USA) as described previously (71). This was performed one day before induction of relapse and at the termination of the experiment on day 45. RotaRod assessment was performed blinded to treatment. Animals were randomised to vehicle or treatment based on their RotaRod scores. Results are expressed as mean ± SEM time that animals maintained rotarod activity. Differences in rota activity; and quantitative neurofilament ELISA was assessed using a Students t test incorporating tests for equality of variance using Sigmaplot (Systat Software, Inc., San Jose, USA) (71).

At the end of the experiment the spinal cord was removed and an enzyme linked immunosorbent assay (ELISA) for heavy chain neurofilament on spinal cord was performed and total nerve content of each spinal cord was estimated following calibration against neurofilament protein standards as described previously (72); (71).

Neurofilament ELISA. Neurofilament level as a validated correlate of spinal cord axonal content as determined by histology was determined as followed. Spinal cords were collected from the spinal columns of untreated (n=11) and JW47 1 mg/kg treated (n=13) animals at the second remission phase of disease post relapse at day 45 post disease induction. Tissues snap frozen and stored at -80ºC prior to homogenisation. Tissues were homogenised in a glass homogeniser in 1ml/100 mg of spinal cord tissue wet weight homogenisation buffer (0.2 mM PMSF, 1mM EDTA, 1mM EGTA, 4M Urea, 10 mM Tris-HCl Sigma UK, pH 7.2,) plus 1:100 HALT protease inhibitor cocktail (Thermo Fisher, UK) and further homogenised by sonication twice for 10 seconds (Cole-Parmer Instruments, USA). Samples were spun down at 13,000 rpm in a bench top centrifuge (Eppendorf, UK) and the supernatant was collected and stored at -80ºC prior to neurofilament determination. Samples were thawed on ice and an enzyme linked immunosorbent assay for heavy chain neurofilament was performed. Briefly, a 96 well plate was coated overnight at 4°C with capture antibody (1:5000 SMI-35 anti-neurofilament H. Covance Inc. Cambridge Bioscience, Cambridge, UK) in coating buffer (0.15M Na_2CO_3, 0.35M $NaHCO_3$, Sigma, UK, pH 9.6. Following one wash in wash buffer (150mM NaCl, 10mM Tris-HCl, 0.1% Tween 20, Sigma, UK pH 7.5), non-specific binding was blocked by incubation with 5% bovine serum albumin (Sigma, UK) in wash buffer for 1 hour at room temperature. Following a wash step, samples and standards (Porcine neurofilament heavy chain, Chemicon International, UK) were diluted in wash buffer with 1% bovine serum albumin and incubated on the plate for 1 hour at room temperature. Following 5 wash steps, the detector antibody was applied (1:1000 rabbit anti-NF200, Sigma, UK) and incubated for a further hour at room temperature. The plate was washed 5 times and the reporter antibody was applied (1:1000 swine anti-rabbit HRP conjugate, DAKO, UK).Following a final 5 washes, tetramethylbenzidine substrate (Sigma, UK) was applied and colour production measured on a BioTek Synergy HT (USA) plate reader at 450nm.

The protein content of the samples was determined by micro-BCA assay (Pierce, Thermo Fisher, UK and axonal neurofilament levels in each were calculated as μg neurofilament per mg of total protein in each sample.

SMI32/SMI35 Ratio. A 96 well plate was coated with either SMI35 anti-phosphorylated Nf-H or SMI32 anti-non-phosphorylated Nf-H which is a marker of axonal damage/dystrophy (Covance Inc. Cambridge Bioscience, Cambridge, UK) antibodies at 1;5000 dilution as above. Due to the nature of the epitope, an absolute standard for SMI32 reactive neurofilaments was unavailable. $Nf\text{-}H^{SMI32}$ was therefore presented as a proportion of total neurofilament as measured by absorbance level and corrected for total protein levels in each sample.

Study approval. All animal procedures were approved by the local ethical review processes and Government Inspectors in accordance with UK Animals (Experimental Procedures) Act 1986, which incorporates directive 2010/63/EU. Experimental details, including: randomisation; powering and blinding, to conform with the ARRIVE (Animals in

Research: Reporting In Vivo Experiments) guidelines have been reported previously (71).

RESULTS

Design and synthesis of a selective CypD inhibitor: We required a molecule with the following profile: a) good CypD potency, b) selectivity for CypD over other cellular cyclophilins by mitochondrial targeting, c) significant brain levels indicating an ability to target MS lesions. d) low immunosuppressive activity and e) a better cytotoxic profile than CsA. CsA is famously non-druglike in terms of small molecule parameters such as Lipinksi's rules of five, however the macrocyclic structure has been proposed to cancel out some of the non-druglike features such as excessive hydrogen bonding (73). In chemical terms the compound is an uncharged, 11 amino acid, macrocyclic peptide. It is lipophilic with a measured logP of 2.7 (74).

A ternary complex of CsA, CypA and calcineurin is required to trigger the immunosuppressive response via inhibition of NFAT dephosphorylation(75). Residues 3-7 are available from the Cyp–cyclosporin complex to bind calcineurin. The ternary complex is closely packed and less tolerant of changes than for Cyp binding alone. The crystal structure of SmBzCsA (Fig. 1*C*) reveals that substitution at the $[Sar]^3$ position does not affect cyclophilin binding but blocks calcineurin binding(76). We chose to modify CsA at the $[Bmt]^1$ side chain where we predicted that substitution would have a similar negative effect on immune-suppression. As the activation of calcineurin is also proposed to mediate some of the cytotoxic effects of CsA we anticipated that selective molecules would improve the toxicity profile while additional selectivity for CypD over the cytoplasmic cyclophilins would provide further gains.

The CsA binding cleft in cyclophilins is highly conserved and mitochondrial targeting provides a convenient way to obtain selectivity for the mitochondrial CypD. A variety of compounds have been suggested to localize to mitochondria. Mostly these are lipophilic cations such as TPP^+, but other cations are known (77). We were attracted by the possibility of utilizing quinolinium cation as a targeting group for several reasons, including its small size, and chemical simplicity. The cation is also present in dequalinium, a topical antibiotic that can also be given in vivo (US4,946,849, Makler, August 7, 1990)(78). We utilized SmBzCsA as a non-immunosuppressive, non-targeted control (Fig. 1*B*)(36,76). We also designed the chemical linker to be small and to be a hydrocarbon chain to minimize any effects on membrane permeabililty.

Synthesis. We employed olefin metathesis as a direct and relatively mild way to alter the natural structure of CsA. The synthesis of the $[Bmt]^1$ linked CsA derivatives is outlined in Fig. 1*A*. Olefin cross-metathesis using the Grubbs-Hoyeda second generation catalyst and the quinolinium substituted olefin yields the target analogue JW47. The synthesis of the required quinolinium olefin is also shown. Shorter linkers did not provide effective couplings in the metathesis reaction (not shown). Synthesis of the fluorescein-PEG-CsA probe for the fluorescence polarization assay was conducted using cross-metathesis, followed by hydrolysis, and successive amide coupling steps to provide the desired compound (Supplementary Fig. S1).

X-ray analysis of a CypD JW47 complex. In order to determine the precise binding mode of JW47 to CypD we determined the X-ray structure of the complex to 1.1 Å resolution. We utilized the protein sequence of CypD (ppif) with a K133I mutation, which enhances crystallisation without significantly affecting activity(48). Crystals were grown with the hanging drop method and the CypD structure 2z6w used as the search model with CsA removed. The electron density for JW47 in the active site is shown (Fig. 2*A*), with the structure of JW47 modelled in green. Crystallographic parameters are shown in Table 1. The core of the macrocycle is almost identical to that of CsA itself while the pendant quinolinium group can adopt two poses (Fig. 2*B*). In both poses the position of the quinolinium group is partially stabilised by crystal contacts with a symmetry related molecule. In one of the poses the1-(pent-4-enyl)quinolinium (salmon colour) extends back over the macrocycle and makes an intramolecular hydrophobic contact with $MeLeu^4$ of JW47. In the other pose (magenta) the 1-(pent-4-enyl)quinolinium moiety extends in the opposite direction to lie along the surface of the CypD making hydrophobic contacts with Ala 103, Gly104, and Pro105.

Cyclophilin enzyme binding. A fluorescence polarization assay was used to determine cyclophilin binding. CsA gives binding constants of Ki 1.4 nM for CypD and 22.5 nM for CypA. These affinities are broadly in agreement with data from other laboratories (59,60). The CsA analogue, SmBzCsA also demonstrated potency in this assay with Ki CypD 236 nM and Ki CypA 202 nM (Table 2) consistent with our data utilizing the classical chymotrypsin based system(36). JW47 showed similar binding to SmBzCsA at Ki CypD 202 nM, and Ki CypA 236 nM. Representative dose response curves for CypD and CypA are shown (Fig. 2*C* and *D*).

The quinolinium group localizes fluorescein to mitochondria. To confirm that quinolinium cation can localize cargo to mitochondria we took a membrane impermeant dye, carboxyfluorescein and conjugated it to mitochondrial using an alkyl linker (Supplementary methods). The linked dye diffused into cells (though some remained extracellularly) and co-localised with tetramethylrhodamine methyl ester demonstrating the mitochondriotropic properties of quinolinium (data not shown).

JW47 is a highly potent inhibitor of Ca^{2+} mediated PT pore formation. In order to assess the efficiency of compounds on Ca^{2+} mediated PT pore formation we measured calcium retention capacity (CRC) of isolated mouse liver mitochondria. The Ca^{2+} concentration in the extra-mitochondrial solution was measured using the membrane impermeable low affinity fluorescent Ca^{2+} sensitive dye Fluo-5N following repeated addition of Ca^{2+} boluses (10 μM). Energised mitochondria take up Ca^{2+}, resulting in a declining fluorescent signal following the Ca^{2+} bolus induced peak. Mitochondria take up and buffer Ca^{2+} up to a threshold when intramitochondrial [Ca^{2+}] reaches threshold to induce PT. This results in loss of mitochondrial membrane potential preventing further Ca^{2+} uptake, resulting in lack of Ca^{2+} buffering, represented by stepwise increase in extramitochondrial [Ca^{2+}] at each Ca^{2+} addition (Fig. 3*A*). The amount of Ca^{2+} required to induce PT characterizes its Ca^{2+} sensitivity and defines mitochondrial CRC. Inhibition of CypD, the Ca^{2+} sensor of PT, thus leads to increased CRC. JW47 inhibited Ca^{2+}-induced PT (i.e. increased CRC) with significantly higher potency as compared to CsA and the non-immunosuppressive inhibitor SmBzCsA. JW47 showed half-maximal inhibition at ~10 nM as compared to ~40nM for CsA in the CRC assay (Fig. 3*B*). These results show that JW47 is approximately a four-fold more potent inhibitor of Ca^{2+} mediated PT pore opening than CsA. In order to confirm that JW47 selectively targets CypD to reduce Ca^{2+} sensitivity of PTP formation, the efficiency of the compound was tested on mitochondria isolated from CypD knockout mice. Neither CsA nor JW47 had any effect on CRC from CypD KO mice (Fig. 3*C*), whereas CRC in the mitochondria from WT mice was significantly increased by both compounds, proving that JW47 inhibits PT pore opening via binding to CypD.

JW47 has a wide safety window over effects on mitochondrial membrane potential or oxidative phosphorylation. To assess the potential adverse effects of JW47, we measured fundamental mitochondrial functional parameters both in cultured rat neurons and in isolated mitochondria, and compared the effects of CsA and JW47 above concentrations causing maximal inhibition of the PT pore (>200 and 40 nM, respectively).

Neither mitochondrial membrane potential (Fig. 4*A*,*B*), oxygen consumption (Fig. 4*C*, *D*) and ATP production (Fig. 4*E*, *F*) were affected by supramaximal JW47 (up to 200 nM) or CsA (up to 1 μM) in either models. JW47 inhibited neuronal mitochondrial membrane potential only at ~25 times higher concentrations (1 μM), as compared to that of its maximal inhibitory effect (40 nM) on the PT pore.

Estimation of cellular CypA activity using an HIV based cellular assay. To test cellular cyclophilin selectivity of JW47 we conducted a human immunodeficiency virus (HIV-1) based cellular assay responsive to CypA inhibition. HIV-1 infection of cell lines can be inhibited by the expression of an artificial antiviral protein, comprising the RBCC domains of owl monkey tripartite motif-containing protein 5 (TRIM5) fused to human CypA (TRIM-CypA). TRIM-CypA inhibited viral infection by 32 fold in the absence of drug (Fig. 5*A*). CsA rescued infectivity through CypA inhibition whereas JW47 rescued infectivity poorly and only at concentrations >10 μM (Fig. 5*B*). A drop to infectivity in non-restricting cells was due to drug toxicity at 5 μM

CsA and above. JW47 showed no evidence for toxicity at any of the concentrations tested.

Activity against drug and anion transporters. The ability of the compounds to affect human pgp (ABCB1) drug transporter activity was assessed using a bioluminescence assay. The standard inhibitor verapamil at 100 µM showed a 40% reduction in luminescence (Fig. 5*C*). Despite being noted as a pgp inhibitor(79) CsA showed only a 16% inhibition at 100 µM. JW47 showed less inhibition than CsA, 8% at 100 µM (Fig. 5*C*). Activity against organic anion transporters OATP1B1 and OATP1B3 has been linked to drug induced unconjugated hyperbilirubinaemia in patients receiving alisoporivir(80). JW47 demonstrated 7 - 8 fold less inhibition of β-estradiol-17-β-D-glucuronide uptake for the OATP1B1 transporter than CsA (2.56 ± 0.47 µM versus 0.44 ± 0.084 µM for CsA). Similarly for the OATP1B3 transporter JW47 showed fourfold less activity than CsA for inhibition of CCK-8 transport (IC_{50} 0.20 ± 0.11versus 0.82 ± 0.07 µM).

Cytotoxicity in HepG2 cells. HepG2 cells represent a convenient model for exploring hepatotoxicity and can be used to estimate multiple cell health parameters simultaneously. JW47 showed less toxicity in all measures examined, most notably cytochrome C release (Fig. 5D).

*Pharmacokinetics***.** JW47 pharmacokinetics was determined in normal ABH mice at 10 mg/kg i.p. at 2 and 4 h. JW47 showed high plasma levels of 10.1 µM at 2 h (Table 3) and appreciable, though much lower brain levels (13.2 nM). A 10 mg/kg dose was used to enable detection in brain. This is broadly comparable with CsA in rodents(79).

JW47 is markedly less immunosuppressive than CsA. The inhibitory effect of JW47 on T cell responses was examined *in vitro*. Concanavalin A and mitogenic CD3/CD28 monoclonal antibodies induce mitogenic T cell proliferative responses that were inhibited by CsA typically in the 1-10 nM range (Fig. 6 panels *A* to *C*). JW47 only exhibited marked immunomodulation in the 1-10 µM range and was cytopathic at 100 µM. Similarly, JW47 exhibited markedly less immunosuppressive activity compared to CsA in an antigen-driven proliferation assay using myelin peptide (myelin oligoglycoprotein residues 35-55) antigen-induced T cell proliferation.

The dominant pathogenic antigen in spinal cord homogenate-induced disease in ABH mice is a hydrophobic residue in proteolipid protein that does not produce robust T cell proliferative responses *in vitro*. Therefore, to identify non-immunosuppressive doses of potential neuroprotective compounds for use in models of MS(14,70) we employed a model using epicutaneous application of the ear skin sensitizer, oxazolone, to induce a T cell proliferative response in the draining auricular lymph node peaking 3 days later (Fig. 7) (70). Dose-response of JW47 in this contact hypersensitivity model showed: daily injection of 1 mg/kg and 0.1 mg/kg i.p. had no effect, while 10 mg/kg i.p. inhibited the T cell response. CsA was immunosuppressive (Fig. 6*D*) at doses known to inhibit T cell proliferation and EAE (70). Daily dosing of 1 mg/kg i.p. JW47 was therefore chosen as a non-immunosuppressive dose for *in vivo* studies.

JW47 induces neuroprotection in vivo and slows the accumulation of disability in an experimental model of multiple sclerosis.
The EAE model of multiple sclerosis can be used to assess both inflammatory and neurodegenerative aspects of the disease (81). It has previously been shown that the severity of neurological disease during disease worsening, associated with weight loss, is directly correlated to the degree of immune infiltration into the spinal cord(81-83). Immunosuppression that inhibits the incidence or severity of disease is usually associated with a reduction in the histological detection of infiltrates, demyelination and axonal loss (81-83).Clinical disease was assessed by scoring neurological signs. In addition to this subjective read-out, objective motor outcomes were detected by assessing loss of motor-co-ordination on an accelerating rotorod, which has previously been shown to exhibit a strong positive correlation with spinal nerve content (71). JW47 was administered daily at 1 mg/kg i.p. shortly before the anticipated onset of relapse. This failed to inhibit the development or the severity of relapse, which would occur with an T cell immunosuppressive agent (84), limited the accumulation of disability due to the inflammatory penumbra (Fig. 8*A*). Thus there were no

differences in the incidence of disease (14/14 JW47 vs. 12/12 vehicle); the onset of induced relapse following injection of SCH in Freunds adjuvant on day 28 (34.5 ± 0.7 days JW47 vs. 34.1 ± 0.8 days vehicle) or maximal severity disease score (3.9 ± 0.1 JW47 vs. 3.9 ± 0.1 vehicle). Animals relapsing during treatment with daily 50mg/kg CsA developed clinical disease with a score of 3.0 ± 0.4 (n=7), which is significantly ($P<0.05$) lower than found with either vehicle of JW47-treatment and is indicative of immunosuppression. Treatment with an immunosuppressive agent, such as 250µg CD4-depleting (YTS191) monoclonal antibody or other immunosuppressive agents, which are optimized for treatment at this late stage will completely eliminate relapse (70). Therefore there was no clinical evidence that JW47 was inducing overt immunosuppression in this paradigm. However, whilst the differences in minimal clinical score during the first remission before treatment were not different (0.6 ± 0.1 JW47 vs. 0.6 ± 0.1 vehicle), following induced-relapse JW47-treated animals accumulated less deficit as a consequence of the attack and demonstrated a significant ($P<0.001$) better recovery during the second remission (minimal neurological score 1.4 ± 0.3 JW47 vs. 3.1 ± 0.1 vehicle ($P<0.001$). This subjective outcome was supported by objective rotarod activity outcomes (Fig. 8*B*). Animals exhibited comparable rotorod activity on day 27 during the first remission (168.8 ± 21.8s JW47 vs. 161.1 ± 16.0s vehicle) but there was significantly ($P<0.001$) less loss of motor co-ordination following treatment with JW47 (Fig. 8*B*). During the second remission after relapse JW47-treated animals maintained activity on an accelerating rotorod for 135.0 ± 42.9s compared to only 46.3 ± 10.1s in vehicle treated animals. This activity strongly correlates with spinal nerve content in this assay (71), and it was found that JW47 lost significantly ($P<0.01$) less nerves(Fig. 8*C*) and axons (Fig. 8*D*) within the spinal cord than vehicle-treated animals, which was measured using a quantitative neurofilament ELISA. The SMI 35 antibody stains neurofilaments with high and low degrees of phosphorylation and reveals thick and thin axons. SMI-32 does not stain thin axons. The degree of neurofilament phosphorylation is modulated by myelination (85) so our readout directly quantifies loss of small axons and by inference demyelination. This assay system has been validated against the histological detection of nerve loss during EAE (72,83) and is a biomarker of neurodegeneration in MS. Thus JW47 exhibits neuroprotective potential and can inhibit loss of nerves due to the inflammatory penumbra during EAE.

Discussion

The permeability transition pore is linked to a necrotic cell death but has been hitherto underexploited as a therapeutic target. The most well-known modulator of the pore, CypD is located on the inner mitochondrial membrane and is resistant to blockade by small molecules. CsA is the standard pan-cyclophilin inhibitor but it shows no selectivity for CypD and exhibits significant cytotoxicity. We have previously shown that CsA can be targeted to mitochondria using the well-known TPP^+ cation. Unfortunately, triphenylphosphonium attached by long alkyl or PEG linkers increases the overall lipophilicity and molecular weight of the conjugate substantially and adversely affects pharmaceutical properties. In this study we utilized quinolinium attached by a short alkyl chain as a mitochondrial targeting cation with a minimal effect on molecular weight and lipophilicity. Olefin cross-metathesis enabled functionalization of CsA using mild conditions which did not affect the sensitive functionality of the cyclic peptide (86). Using this methodology we identified JW47 as a prototype inhibitor. In isolated mitochondria, JW47 delayed opening of the PT pore and was more active than CsA. Detailed measures of oxidative phosphorylation indicated that JW47 only affected cellular ATP production at supramaximal concentrations but not at the effective concentration (40nM), or the lowest maximally effective concentration (200 nM). In cortical neurons, mitochondria were not affected by 40nM JW47, but were significantly depolarized by 1µM JW47. The greater effect of JW47 in mitochondrial Ca^{2+} buffering compared to CsA indicates that quinolinium is effective in directing the drug to mitochondria in accordance with its more negative electro-potential and in agreement with the Nernst equation(87). JW47 has less intrinsic CypD binding than CsA, but is a more potent PT pore inhibitor. In addition, in isolated mitochondria from CypD knock out mice, JW47 had no effect on Ca^{2+} mediated PT, proving

that its principal mechanism of action is mediated by CypD binding. In a system designed to detect restriction of HIV replication via CypA JW47 showed no activity in contrast to both CsA and SmBzCsA indicating that JW47 has minimal ability to inhibit CypA in cells. Drug transporter studies on JW47 indicate less propensity to cause bilirubinemia via inhibition of the bilirubin transporter OATP1B1 in comparison to CsA itself and an analogue Alisporivir(88). A multi-parameter study of JW47 in hepatocellular carcinoma derived HepG2 cells showed less toxicity than CsA (89) with perhaps a surprising drop in mitochondrial toxicity, despite the expected sequestration of the ligand to mitochondria (88)

EAE is a T cell-mediated, autoimmune model of MS, which can develop relapsing autoimmunity and progressive neurodegeneration (20,81,84) 88 should be 84. Studies using transgenic mice in the EAE model have shown that the PT pore pathway can determine neurodegeneration, independently of the peripheral immune response (20,21,90). Whilst CsA can prophylactically inhibit the generation of EAE, it is therapeutically less effective during spontaneous-relapsing EAE and was did not inhibit relapsing MS also (70,91). Furthermore, the nephrotoxicity of CsA also limited its clinical utility in MS (39). Progressive MS, is associated the accumulation of nerve loss and disability, shows minimal response to peripheral immunosuppression and is currently untreatable (92). It was found that doses of JW47 could be selected to induce neuroprotection without causing overt T cell immunosuppression We chose ELISA detection of total spinal cord nerve content as a robust non-biased way to fully quantify nerve loss (and by implication myelin content). This protection may be via direct effects on nerves, although it is possible that JW47 also exhibited some influence on innate inflammatory cells, which are believed to drive progressive neurodegeneration. The level of efficacy of Jw47 is similar to that found previously with other neuroprotective agents in this experimental paradigm (14), which appear to have some predictive value for identifying neuroprotective agents in multiple sclerosis(14,93). Relapsing disease was not inhibited with JW47, in contrast to that, which would occur following T cell immunosuppression with drugs used to treat relapsing neuroimmunological disease (94). These current agents do not however stop progressive neurodegeneration (92) and therefore it is believed that drugs like JW47 should be used in combination with current immunosuppressive disease modifying drugs to target the neurodegenerative effects that are currently not treated.

It is therefore of interest that CsA-treatment showed some modest benefit in progressive MS(39), and in neuromyelitis optica, another immune-mediated demyelinating disease(95). This suggests that inhibition of CypD activity in humans may offer some clinical benefit and would benefit from delivery of a CypD selective inhibitor. We anticipate that JW47, which is more selective and less toxic in cells would be better tolerated than CsA *in vivo*.

CsA is thought to be excluded from the CNS by adenosine binding cassette drug transporters, such as an ABCB1, ABCC1, ABCC4 and ABCG2 which are present in the brain (14,96,97). JW47 exhibited limited activity as ABCB1 substrate compared to CsA and could be detected in the brain of normal animals. A pharmacokinetic experiment with JW47 showed potential for *in vivo* evaluation with high plasma levels of JW47 that are within the active *in vitro* dose range and significant though lower brain levels. Whilst brain levels may be higher at $C_{max,}$ it is also probable that brain levels and importantly spinal cord levels may be significantly higher in animals with active and chronic EAE, which exhibit mainly spinal cord disease, due to alterations in metabolism and blood-brain barrier breakdown that occurs in EAE and MS (11,71,98). Furthermore, CNS adenosine binding cassette drug transporters, notably p-glycoprotein (ABCB1) are down-regulated from vasculature such that compounds, even ABCB1-substrates, can be selectively targeted to lesions, despite poor apparent global CNS penetration (14). Further studies to determine the oral bioavailability, pharmacokinetic/ pharmacodynamics and toxicology of JW47 and related molecules are warranted. The action of JW47 demonstrates that pharmacological inhibitors of the PT pore are neuroprotective in EAE, as predicted using genetic ablation studies of CypD (20) and P66ShcA in the PT pore pathway (21,99) and may provide a

treatment for neurodegeneration and progression of disability during relapsing–remitting and progressive MS and other neurological diseases.

In summary we have shown that quinolinium is an effective mitochondrial targeting group, the CsA tagged molecule is less cytotoxic than CsA and shows little ability to interact with cytoplasmic proteins. In mitochondria JW47 is a more potent inhibitor of pore opening than CsA, and does not affect mitochondrial function at a concentration of maximal inhibition. Furthermore JW47 demonstrates a pronounced neuroprotective effect in vivo and should be a useful tool for investigation of the role of the PT pore in other neurodegenerative conditions and in models of ischaemia–reperfusion injury. The quinolinium cation is smaller and is more amenable to pharmaceutical optimization than TPP^+ and we anticipate that it will become a useful addition to the toolbox of mitochondrial targeting groups.

Acknowledgements: The authors acknowledge the support of FastForward, National Multiple Sclerosis Society. JH is funded by a studentship from Eisai UK Ltd. Diamond Light Source for access to beamline I04 (proposal no. mx8922). GS is supported by the British Heart Foundation, Wellcome Trust, Telethon Italy and the Italian Association for Cancer Research (AIRC). Wellcome Trust Senior Fellowship 090940 to G.J.T., the Medical Research Council, an MRC Confidence in Concept Award to G.J.T. and D.S. and the National Institute for Health Research (NIHR) University College London Hospitals Biomedical Research Centre. DLS would like to thank Prof Martin Crompton for inspiring this project, and we thank D. Housenloy and S. Davidson for providing the CypD -/- animals.

Conflict of interest: The authors (DLS, DB) declare competing financial interests.

Author contributions: JW, MIS and DS synthesized the compounds. XS and AC determined the X-ray structure. GP and DB did the pgp and *in vivo* work. FL and FP did the immunoassays and in vivo immunosuppression studies. JH and GP performed the mitochondrial Ca^{2+} buffering assays and the mitochondrial functional assays, devised, supervised and directed by GS and MRD. MK and JW did the Cyp assays. LH did the cellular HIV assay. DB, DLS obtained funding for the study MRD, GS, GT, DB, and DLS wrote initial drafts of the paper. All authors contributed to the final manuscript

References

1. Giorgio, V., von Stockum, S., Antoniel, M., Fabbro, A., Fogolari, F., Forte, M., Glick, G. D., Petronilli, V., Zoratti, M., Szabo, I., Lippe, G., and Bernardi, P. (2013) *Proceedings of the National Academy of Sciences of the United States of America* **110**, 5887-5892
2. Alavian, K. N., Beutner, G., Lazrove, E., Sacchetti, S., Park, H. A., Licznerski, P., Li, H., Nabili, P., Hockensmith, K., Graham, M., Porter, G. A., Jr., and Jonas, E. A. (2014) *Proceedings of the National Academy of Sciences of the United States of America* **111**, 10580-10585
3. Bonora, M., Bononi, A., De Marchi, E., Giorgi, C., Lebiedzinska, M., Marchi, S., Patergnani, S., Rimessi, A., Suski, J. M., Wojtala, A., Wieckowski, M. R., Kroemer, G., Galluzzi, L., and Pinton, P. (2013) *Cell Cycle* **12**, 674-683
4. Halestrap, A. P., and Richardson, A. P. (2015) *Journal of molecular and cellular cardiology* **78**, 129-141
5. Giorgio, V., Bisetto, E., Soriano, M. E., Dabbeni-Sala, F., Basso, E., Petronilli, V., Forte, M. A., Bernardi, P., and Lippe, G. (2009) *The Journal of biological chemistry* **284**, 33982-33988

6. Chinopoulos, C., Konrad, C., Kiss, G., Metelkin, E., Torocsik, B., Zhang, S. F., and Starkov, A. A. (2011) *The FEBS journal* **278**, 1112-1125
7. Basso, E., Petronilli, V., Forte, M. A., and Bernardi, P. (2008) *The Journal of biological chemistry* **283**, 26307-26311
8. Compston, A., and Coles, A. (2008) *Lancet* **372**, 1502-1517
9. Marta, M., and Giovannoni, G. (2012) *CNS & neurological disorders drug targets* **11**, 610-623
10. Trapp, B. D., Peterson, J., Ransohoff, R. M., Rudick, R., Mork, S., and Bo, L. (1998) *The New England journal of medicine* **338**, 278-285
11. Kutzelnigg, A., and Lassmann, H. (2014) *Handbook of clinical neurology* **122**, 15-58
12. Campbell, G. R., Worrall, J. T., and Mahad, D. J. (2014) *Mult Scler*
13. Ohno, N., Chiang, H., Mahad, D. J., Kidd, G. J., Liu, L., Ransohoff, R. M., Sheng, Z. H., Komuro, H., and Trapp, B. D. (2014) *Proceedings of the National Academy of Sciences of the United States of America* **111**, 9953-9958
14. Al-Izki, S., Pryce, G., Hankey, D. J., Lidster, K., von Kutzleben, S. M., Browne, L., Clutterbuck, L., Posada, C., Edith Chan, A. W., Amor, S., Perkins, V., Gerritsen, W. H., Ummenthum, K., Peferoen-Baert, R., van der Valk, P., Montoya, A., Joel, S. P., Garthwaite, J., Giovannoni, G., Selwood, D. L., and Baker, D. (2014) *Brain : a journal of neurology* **137**, 92-108
15. Barrientos, S. A., Martinez, N. W., Yoo, S., Jara, J. S., Zamorano, S., Hetz, C., Twiss, J. L., Alvarez, J., and Court, F. A. (2011) *The Journal of neuroscience : the official journal of the Society for Neuroscience* **31**, 966-978
16. Dutta, R., McDonough, J., Yin, X., Peterson, J., Chang, A., Torres, T., Gudz, T., Macklin, W. B., Lewis, D. A., Fox, R. J., Rudick, R., Mirnics, K., and Trapp, B. D. (2006) *Annals of neurology* **59**, 478-489
17. Mahad, D., Ziabreva, I., Lassmann, H., and Turnbull, D. (2008) *Brain : a journal of neurology* **131**, 1722-1735
18. Kapoor, R., Davies, M., Blaker, P. A., Hall, S. M., and Smith, K. J. (2003) *Annals of neurology* **53**, 174-180
19. Hazelton, J. L., Petrasheuskaya, M., Fiskum, G., and Kristian, T. (2009) *Journal of neuroscience research* **87**, 1250-1259
20. Forte, M., Gold, B. G., Marracci, G., Chaudhary, P., Basso, E., Johnsen, D., Yu, X., Fowlkes, J., Rahder, M., Stem, K., Bernardi, P., and Bourdette, D. (2007) *Proceedings of the National Academy of Sciences of the United States of America* **104**, 7558-7563
21. Savino, C., Pelicci, P., and Giorgio, M. (2013) *Oxidative medicine and cellular longevity* **2013**, 719407
22. Mbye, L. H., Singh, I. N., Sullivan, P. G., Springer, J. E., and Hall, E. D. (2008) *Experimental neurology* **209**, 243-253
23. Hanell, A., Greer, J. E., McGinn, M. J., and Povlishock, J. T. (2015) *Acta neuropathologica* **129**, 317-332
24. Guo, L., Du, H., Yan, S., Wu, X., McKhann, G. M., Chen, J. X., and Yan, S. S. (2013) *PloS one* **8**, e54914
25. Du, H., Guo, L., Zhang, W., Rydzewska, M., and Yan, S. (2011) *Neurobiology of aging* **32**, 398-406
26. Martin, L. J., Semenkow, S., Hanaford, A., and Wong, M. (2014) *Neurobiology of aging* **35**, 1132-1152

27. Martin, L. J., Gertz, B., Pan, Y., Price, A. C., Molkentin, J. D., and Chang, Q. (2009) *Experimental neurology* **218**, 333-346
28. Quintanilla, R. A., Jin, Y. N., von Bernhardi, R., and Johnson, G. V. (2013) *Molecular neurodegeneration* **8**, 45
29. Reddy, P. H., Tripathi, R., Troung, Q., Tirumala, K., Reddy, T. P., Anekonda, V., Shirendeb, U. P., Calkins, M. J., Reddy, A. P., Mao, P., and Manczak, M. (2012) *Biochimica et biophysica acta* **1822**, 639-649
30. Readnower, R. D., Pandya, J. D., McEwen, M. L., Pauly, J. R., Springer, J. E., and Sullivan, P. G. (2011) *Journal of neurotrauma* **28**, 1845-1853
31. Nakagawa, T., Shimizu, S., Watanabe, T., Yamaguchi, O., Otsu, K., Yamagata, H., Inohara, H., Kubo, T., and Tsujimoto, Y. (2005) *Nature* **434**, 652-658
32. Baines, C. P., Kaiser, R. A., Purcell, N. H., Blair, N. S., Osinska, H., Hambleton, M. A., Brunskill, E. W., Sayen, M. R., Gottlieb, R. A., Dorn, G. W., Robbins, J., and Molkentin, J. D. (2005) *Nature* **434**, 658-662
33. Kato, M., Akao, M., Matsumoto-Ida, M., Makiyama, T., Iguchi, M., Takeda, T., Shimizu, S., and Kita, T. (2009) *Cardiovascular research* **83**, 335-344
34. Wu, N., Li, W. N., Shu, W. Q., Lv, Y., and Jia, D. L. (2015) *European review for medical and pharmacological sciences* **19**, 446-454
35. Barbarino, J. M., Staatz, C. E., Venkataramanan, R., Klein, T. E., and Altman, R. B. (2013) *Pharmacogenetics and genomics* **23**, 563-585
36. Malouitre, S., Dube, H., Selwood, D., and Crompton, M. (2010) *The Biochemical journal* **425**, 137-148
37. Davis, T. L., Walker, J. R., Campagna-Slater, V., Finerty, P. J., Paramanathan, R., Bernstein, G., MacKenzie, F., Tempel, W., Ouyang, H., Lee, W. H., Eisenmesser, E. Z., and Dhe-Paganon, S. (2010) *PLoS biology* **8**, e1000439
38. Gogarten, W., Van Aken, H., Moskopp, D., Roos, N., Schleef, J., Marcus, M., and Meyer, J. (1998) *Journal of neurosurgical anesthesiology* **10**, 101-105
39. Scheinberg, L. C. (1990) *Annals of neurology* **27**, 591-605
40. Hecking, M., Kainz, A., Schillinger, M., Posch, C., Birsan, T., Rasoul-Rockenschaub, S., Bohmig, G. A., Schmaldienst, S., Watschinger, B., Horl, W. H., Muhlbacher, F., and Saemann, M. D. (2008) *Transplant international : official journal of the European Society for Organ Transplantation* **21**, 223-233
41. Ross, M. F., Kelso, G. F., Blaikie, F. H., James, A. M., Cocheme, H. M., Filipovska, A., Da Ros, T., Hurd, T. R., Smith, R. A., and Murphy, M. P. (2005) *Biochemistry. Biokhimiia* **70**, 222-230
42. Gane, E. J., Weilert, F., Orr, D. W., Keogh, G. F., Gibson, M., Lockhart, M. M., Frampton, C. M., Taylor, K. M., Smith, R. A., and Murphy, M. P. (2010) *Liver international : official journal of the International Association for the Study of the Liver* **30**, 1019-1026
43. Millard, M., Pathania, D., Shabaik, Y., Taheri, L., Deng, J., and Neamati, N. (2010) *PloS one* **5**
44. Leo, S., Szabadkai, G., and Rizzuto, R. (2008) *Annals of the New York Academy of Sciences* **1147**, 264-274
45. Reily, C., Mitchell, T., Chacko, B. K., Benavides, G., Murphy, M. P., and Darley-Usmar, V. (2013) *Redox biology* **1**, 86-93
46. Porteous, C. M., Menon, D. K., Aigbirhio, F. I., Smith, R. A., and Murphy, M. P. (2013) *Biochimica et biophysica acta* **1830**, 3458-3465

47. Dube, H., Selwood, D., Malouitre, S., Capano, M., Simone, M. I., and Crompton, M. (2012) *The Biochemical journal* **441**, 901-907
48. Schlatter, D., Thoma, R., Kung, E., Stihle, M., Muller, F., Borroni, E., Cesura, A., and Hennig, M. (2005) *Acta crystallographica. Section D, Biological crystallography* **61**, 513-519
49. Valasani, K. R., Carlson, E. A., Battaile, K. P., Bisson, A., Wang, C., Lovell, S., and ShiDu Yan, S. (2014) *Acta crystallographica. Section F, Structural biology communications* **70**, 717-722
50. Kajitani, K., Fujihashi, M., Kobayashi, Y., Shimizu, S., Tsujimoto, Y., and Miki, K. (2008) *Proteins* **70**, 1635-1639
51. McCoy, A. J., Grosse-Kunstleve, R. W., Adams, P. D., Winn, M. D., Storoni, L. C., and Read, R. J. (2007) *Journal of applied crystallography* **40**, 658-674
52. Winn, M. D., Ballard, C. C., Cowtan, K. D., Dodson, E. J., Emsley, P., Evans, P. R., Keegan, R. M., Krissinel, E. B., Leslie, A. G., McCoy, A., McNicholas, S. J., Murshudov, G. N., Pannu, N. S., Potterton, E. A., Powell, H. R., Read, R. J., Vagin, A., and Wilson, K. S. (2011) *Acta crystallographica. Section D, Biological crystallography* **67**, 235-242
53. Murshudov, G. N., Vagin, A. A., and Dodson, E. J. (1997) *Acta crystallographica. Section D, Biological crystallography* **53**, 240-255
54. Vagin, A. A., Steiner, R. A., Lebedev, A. A., Potterton, L., McNicholas, S., Long, F., and Murshudov, G. N. (2004) *Acta crystallographica. Section D, Biological crystallography* **60**, 2184-2195
55. Emsley, P., and Cowtan, K. (2004) *Acta crystallographica. Section D, Biological crystallography* **60**, 2126-2132
56. Schuttelkopf, A. W., and van Aalten, D. M. (2004) *Acta crystallographica. Section D, Biological crystallography* **60**, 1355-1363
57. Laskowski, R. A., MacArthur, M. W., Moss, D. S., and Thornton, J. M. (1993) *Journal of applied crystallography* **26**, 9
58. Davis, I. W., Leaver-Fay, A., Chen, V. B., Block, J. N., Kapral, G. J., Wang, X., Murray, L. W., Arendall, W. B., 3rd, Snoeyink, J., Richardson, J. S., and Richardson, D. C. (2007) *Nucleic acids research* **35**, W375-383
59. Gaali, S., Kozany, C., Hoogeland, B., Klein, M., and Hausch, F. (2010) *ACS medicinal chemistry letters* **1**, 536-539
60. Liu, Y., Jiang, J., Richardson, P. L., Reddy, R. D., Johnson, D. D., and Kati, W. M. (2006) *Analytical biochemistry* **356**, 100-107
61. Nikolovska-Coleska, Z., Wang, R., Fang, X., Pan, H., Tomita, Y., Li, P., Roller, P. P., Krajewski, K., Saito, N. G., Stuckey, J. A., and Wang, S. (2004) *Analytical biochemistry* **332**, 261-273
62. Astin, R., Bentham, R., Djafarzadeh, S., Horscroft, J. A., Kuc, R. E., Leung, P. S., Skipworth, J. R., Vicencio, J. M., Davenport, A. P., Murray, A. J., Takala, J., Jakob, S. M., Montgomery, H., and Szabadkai, G. (2013) *Scientific reports* **3**, 2467
63. Lim, S. Y., Hausenloy, D. J., Arjun, S., Price, A. N., Davidson, S. M., Lythgoe, M. F., and Yellon, D. M. (2011) *Journal of cellular and molecular medicine* **15**, 2443-2451
64. Naldini, L., Blömer, U., Gallay, P., Ory, D., Mulligan, R., Gage, F. H., Verma, I. M., and Trono, D. (1996) *Science* **272**, 263-267
65. Zufferey, R., Nagy, D., Mandel, R. J., Naldini, L., and Trono, D. (1997) *Nature Biotech* **15**, 871-875

66. Bainbridge, J. W., Stephens, C., Parsley, K., Demaison, C., Halfyard, A., Thrasher, A. J., and Ali, R. R. (2001) *Gene therapy* **8**, 1665-1668.
67. Ylinen, L. M., Price, A. J., Rasaiyaah, J., Hue, S., Rose, N. J., Marzetta, F., James, L. C., and Towers, G. J. (2010) *PLoS pathogens* **6**, e1001062
68. McEwan, W. A., Schaller, T., Ylinen, L. M., Hosie, M. J., Towers, G. J., and Willett, B. J. (2009) *Journal of virology* **83**, 8270-8275
69. Amor, S., Groome, N., Linington, C., Morris, M. M., Dornmair, K., Gardinier, M. V., Matthieu, J. M., and Baker, D. (1994) *J Immunol* **153**, 4349-4356
70. O'Neill, J. K., Baker, D., Davison, A. N., Maggon, K. K., Jaffee, B. D., and Turk, J. L. (1992) *Journal of neuroimmunology* **38**, 53-62
71. Al-Izki, S., Pryce, O'Neill J. K, Butter, C., Giovannoni, G., Amor, S., and Baker, D. (2012) *Mult Scler Rel Dis* **1**, 29-38
72. Jackson, S. J., Pryce, G., Diemel, L. T., Cuzner, M. L., and Baker, D. (2005) *Neuroscience* **134**, 261-268
73. Macarron, R., and Luengo, J. I. (2011) *Future medicinal chemistry* **3**, 505-507
74. Sharma, P., Varma, M. V., Chawla, H. P., and Panchagnula, R. (2005) *Farmaco* **60**, 870-873
75. Hogan, P. G., Chen, L., Nardone, J., and Rao, A. (2003) *Genes & development* **17**, 2205-2232
76. Rasaiyaah, J., Tan, C. P., Fletcher, A. J., Price, A. J., Blondeau, C., Hilditch, L., Jacques, D. A., Selwood, D. L., James, L. C., Noursadeghi, M., and Towers, G. J. (2013) *Nature* **503**, 402-405
77. Hoye, A. T., Davoren, J. E., Wipf, P., Fink, M. P., and Kagan, V. E. (2008) *Accounts of chemical research* **41**, 87-97
78. Rodrigues, J. R., and Gamboa de Dominguez, N. (2007) *Experimental parasitology* **115**, 19-24
79. Schinkel, A. H., Wagenaar, E., van Deemter, L., Mol, C. A., and Borst, P. (1995) *The Journal of clinical investigation* **96**, 1698-1705
80. Templeton, I., Eichenbaum, G., Sane, R., and Zhou, J. (2014) *Methods Mol Biol* **1113**, 471-483
81. Hampton, D. W., Serio, A., Pryce, G., Al-Izki, S., Franklin, R. J., Giovannoni, G., Baker, D., and Chandran, S. (2013) *Acta neuropathologica communications* **1**, 84
82. Allen, S. J., Baker, D., O'Neill, J. K., Davison, A. N., and Turk, J. L. (1993) *Cellular immunology* **146**, 335-350
83. Jackson, S. J., Lee, J., Nikodemova, M., Fabry, Z., and Duncan, I. D. (2009) *Journal of neuropathology and experimental neurology* **68**, 616-625
84. Baker, D., Gerritsen, W., Rundle, J., and Amor, S. (2011) *Mult Scler* **17**, 647-657
85. Starr, R., Attema, B., DeVries, G. H., and Monteiro, M. J. (1996) *Journal of neuroscience research* **44**, 328-337
86. Smulik, J. A., Diver, S. T., Pan, F., and Liu, J. O. (2002) *Organic letters* **4**, 2051-2054
87. Lemasters, J. J., and Ramshesh, V. K. (2007) *Methods in cell biology* **80**, 283-295
88. Gallay, P. A., and Lin, K. (2013) *Drug design, development and therapy* **7**, 105-115
89. Chung, N. S., and Wasan, K. M. (2004) *Advanced drug delivery reviews* **56**, 1315-1334
90. Su, K. G., Savino, C., Marracci, G., Chaudhary, P., Yu, X., Morris, B., Galipeau, D., Giorgio, M., Forte, M., and Bourdette, D. (2012) *The European journal of neuroscience* **35**, 562-571

91. Kappos, L., Patzold, U., Dommasch, D., Poser, S., Haas, J., Krauseneck, P., Malin, J. P., Fierz, W., Graffenried, B. U., and Gugerli, U. S. (1988) *Annals of neurology* **23**, 56-63
92. Coles, A. J., Wing, M. G., Molyneux, P., Paolillo, A., Davie, C. M., Hale, G., Miller, D., Waldmann, H., and Compston, A. (1999) *Annals of neurology* **46**, 296-304
93. Raftopoulos, R., Rangarajan, A., Chen, C.-L., Hickman, S., Toosy, A., Wheeler-Kingshott, C. A., Altmann, D., Malik, S., Paling, D., Yiannakas, M., Schmierer, K., Sharrack, B., Sheridan, R., Giovannoni, G., Balcer, L., Miller, D., Ishikawa, H., and Kapoor, R. (2015) *Mult Scler* **23**, 273
94. Pryce, G., O'Neill, J. K., Croxford, J. L., Amor, S., Hankey, D. J., East, E., Giovannoni, G., and Baker, D. (2005) *Journal of neuroimmunology* **165**, 41-52
95. Kageyama, T., Komori, M., Miyamoto, K., Ozaki, A., Suenaga, T., Takahashi, R., Kusunoki, S., Matsumoto, S., and Kondo, T. (2013) *Journal of neurology* **260**, 627-634
96. Bart, J., Groen, H. J., Hendrikse, N. H., van der Graaf, W. T., Vaalburg, W., and de Vries, E. G. (2000) *Cancer treatment reviews* **26**, 449-462
97. Pryce, G., Visintin, C., Ramagopalan, S. V., Al-Izki, S., De Faveri, L. E., Nuamah, R. A., Mein, C. A., Montpetit, A., Hardcastle, A. J., Kooij, G., de Vries, H. E., Amor, S., Thomas, S. A., Ledent, C., Marsicano, G., Lutz, B., Thompson, A. J., Selwood, D. L., Giovannoni, G., and Baker, D. (2014) *FASEB journal : official publication of the Federation of American Societies for Experimental Biology* **28**, 117-130
98. Al-Izki, S., Pryce, G., O'Neill, J. K., Butter, C., Giovannoni, G., Amor, S., and Baker, D. (2012) *Multiple Sclerosis and Related Disorders* **1**, 29-38
99. Su, K., Bourdette, D., and Forte, M. (2013) *Frontiers in physiology* **4**, 169

FOOTNOTES

The abbreviations used are: CRC, calcium retention capacity; CypD, cyclophilin D; CypA, cyclophilin A; CsA, cyclosporine; FP, EAE, experimental autoimmune encephalomyelitis fluorescence polarization; PT, permeability transition; MS, multiple sclerosis; TPP^+, triphenylphosphonium.

FIGURE LEGENDS

Figure 1. *A* Synthesis of [Bmt-1] and [Sar-3] substituted analogues by olefin Cross-metathesis and alkylation. Reagents i) DCM, Hoveyda-Grubbs catalyst, 2nd generation, reflux, 30 hr. ii) LDA, allyl bromide. B Structure of SmBzCsA, *C* The crystal structure of SmBzCsA (pdb code 4IPZ) is shown bound to CypA (solid magenta surface). The aligned structure of CypD (pdb code 5a0e) is shown as a wire mesh. Amino acids 9 to 2 are involved in cyclophilin binding. The [Bmt]1 residue (pink) side chain and the [Sar]3 substituent do not affect cyclophilin binding.

Figure 2. *A* Crystal structure of JW47 in complex with CypD and its effect on Ca^{2+} induced PT., electron density of JW47 in the CypD catalytic site is shown as a wire mesh with JW47 modelled into the density as a ball and stick model (green). ***B***, JW47 adopts two poses in the crystal structure shown in orange and magenta. The orange pose illustrates a possible stabilizing interaction with Ala103, Pro105, and Lys125. Surface in green is generated from the chain that co-crystallised with this pose. Note that Lys125 also adopts 2 conformations. *C* Fluorescence polarization assay for cyclophilin binding obtained using a fluorescein labeled CsA probe. Typical data for CypD is shown. The concentration of the probe is 45 nM and the enzyme 40 nM. mP values are fitted to a dose response curve using Origin. *D* Fluorescence polarization data for CypA.

Figure 3 ***A***. Comparison of the effect of JW47, CsA and SmBzCsA on mitochondrial Ca^{2+} retention capacity (CRC). Representative traces of the Ca^{2+} retention capacity assay in isolated rat liver mitochondria. Fluo-5N fluorescence was measured in the extramitochondrial solution following repeated additions of Ca^{2+} (10 µM, for details see Materials and Methods). Increase in fluorescence indicates loss of Ca^{2+} retention due to PT pore opening. Inhibition of PT pore with different compounds (added at 200 nM) increases CRC, represented by the delay in increase of fluorescence. ***B***. Dose response curves of JW47 and CsA on PT inhibition (expressed as % increase in CRC compared to DMSO treatment). ***C***. Quantification of the dose dependent effects of CsA and JW47 on CRC (PT) in liver mitochondria isolated from WT and CypD KO animals. Percentage inhibition denotes increase in CRC compared to DMSO treatment, normalised to WT. * $p < 0.05$ (t-test)

Figure 4. Mitochondrial and cellular toxicological assessment of JW47 and CsA.
Mitochondrial parameters were measured in rat cortical neurons (***A, E***) and isolated rat liver mitochondria (**B-D, F**). ***A, B***:Mitochondrial membrane potential was measured in tetramethyl-rhodamine methylesther (TMRM) loaded neurons using ImageXpress MicroXL in (**A**) and rhodamine-123 loaded isolated mitochondria using a fluorescent plate reader in (***B***). Values in are normalised to DMSO (100%) and FCCP (2 µM, 0%) treated samples. * $p < 0.05$ (one way ANOVA) ***C, D***: O_2 consumption was measured in mitochondria isolated from rat liver in the presence of glutamate and malate using Oroboros high resolution oxygraph as described in Methods. The effect of compounds on basal, leak (oligomycin, 2.5 µM) and maximal uncoupled respiration (FCCP, titrated to give maximum effect) is shown, as compared to basal, DMSO controls. * $p < 0.05$ (paired t-tests). ***E, F*:** ATP levels in cortical neurons (***E***) and ATP production of isolated mitochondria in the presence of substrates and ADP ***(F***) was measured using a luciferase assay as described in Methods. Iodoacetic acid (IAA, 1 mM) and oligomycin (oligo, 2.5 µM) was used to show the contribution of glycolysis and mitochondrial ATP synthesis, respectively. * $p < 0.05$ (t-test). (***G***) In vitro toxicological assessment of CsA and JW47. HepG2 cells were plated and after 24 hr the cells were treated with the compounds at a range of concentrations. At the end of the incubation period, the cells were loaded with the relevant dye/antibody for each cell health marker and scanned (see Methods). Data are shown as EC_{50} values (µM) ± R^2, # = no reponse observed at 100 µM

Figure 5: Assessment of in cell CypA binding. CRFK cells transduced with either empty vector (filled squares) or TRIM-CypA (open circles) were infected with VSV-pseudotyped GFP-expressing HIV-1 vector, in the presence of DMSO or increasing concentration of drug. ***A*** CsA, ***B***. JW47. Viral infection was measured by flow cytometry at 48 hr post infection. Data are the average of three independent experiments. *C*, P-glycoprotein drug transporter activity. Vehicle, verapamil (100 µM) and CsA analogues were tested as substrates for p-glycoprotein (Pgp-Glow assay). Results are the mean ± SEM bioluminescence measurements from the luciferin reporter.

Figure 6: The oxazolone contact hypersensitivity test. A low severity in vivo measure of T cell proliferation, is used as a rapid screen for immunosuppressive doses of agents. Oxazolone administered to the ear induces an increase in cell number and proliferation in the draining auricular lymph node

Figure 7: JW47 exhibits less immunosuppressive activity than CsA. Mitogenesis in vitro, 4 x 10^{-5} cells normal mouse splenocytes were incubated with ***A*** 5µg/ml concanavalin A ***B*** Mitogenic CD3/CD28 monoclonal antibodies or ***C*** splenocytes from MOG residues 35-55 peptide immunized mice in the presence of 5µg/ml MOG peptide with vehicle or compounds for ***A,B*** 2 or 4 ***C*** days prior to the addition of 1 µCi ^{3}H-thymidine and were harvested 16-20h later and tritiated thymidine incorporation was assessed by beta scintillation counting. The results represent the mean ± SEM of triplicate samples.
D Low doses of JW47 in vivo exhibited no immunosuppressive activity. 25 µl of 2.5% Oxazolone (OX) or acetone: olive oil (4:1) vehicle (AOO) was applied to the ear skin of ABH mice on day 0. On day 3 the draining auricular lymph nodes of 3-4 mice/group were removed and 5 x 10^5 cells were cultured overnight

in the presence of 1μ Ci ^{3}H-thymidine. Animals were treated with 0.1 ml vehicle or 0.1-10 mg/kg JW47 or 50 mg/kg CsA. The results represent the mean ± SEM of at least quadruplicate samples.

Figure 8. JW47 limits the accumulation of neurodegeneration and disability during relapsing autoimmune encephalomyelitis. ABH mice were injected with SCH in Freund's complete adjuvant on day 0 and 7 to induce paralytic EAE. A relapse was induced on day 28 during the first remission, using a further injection of SCH in Freund's incomplete adjuvant. Animals were treated daily from day 33 onwards with either 1 mg/kg i.p. JW47 (black diamonds. n =14) in ethanol: cremophor: PBS (1:1:18) or vehicle (Grey circles. n=12). The results represent ***A*** the mean daily neurological score ± SEM; ***B*** the mean rotarod activity representing the mean ± SEM time before falling/failing to stay on an accelerating rotarod before (on day 27) or after (on day 45) treatment with either vehicle (Grey bar) or JW47 (Black bar). *** P<0.001 compared to vehicle treatment. ***C*** Axonal content in the spinal cord following treatment of relapsing EAE with JW47 1 mg/kg measured as neurofilament level adjusted for total protein content. EAE was induced with spinal cord homogenate in complete Freund's adjuvant on days 0 and 7 and a relapse was induced by re-immunisation with spinal cord homogenate in complete Freund's adjuvant at day 28. Animals were randomized according to RotaRod performance score at day 27 to receive either vehicle (Cremophor (Sigma, UK), alcohol, phosphate buffered saline 1:1;18) or 1mg/kg i.p JW47 from day 33 p.i. just prior to the development of relapse at day 35 until day 47. Animals were killed and the spinal cords removed using hydrostatic pressure and axonal content measured using a quantitative neurofilament-specific ELISA. n=11 untreated, n=13 JW47 treated. Ratio of dephosphorylated (SMI-32 reactive) neurofilament to hyperphosphorylated (SMI-35 reactive) neurofilament as measured by ELISA in spinal cord homogenates from untreated post-relapse untreated animals; n=11 or JW47 1 mg/kg treated animals n=13 *** P<0.001 adjusted for total protein level.

Table 1. Crystallographic statistics of JW47

Space group	$P2_12_12_1$
Cell dimensions	
a (Å)	38.12
b (Å)	69.51
c (Å)	109.17
Mathews Coefficient	2.03
Data Statistics	**All data**
Resolution (Å)	35.99-1.08 (1.11-1.08)
No. measurements	1255737 (13170)
No. unique reflections	101679 (2352)
Completeness (%)	81.5 (24.7)
R_{meas}	0.061 (1.279)
R_{pim}	0.017 (0.518)
I/ϭ(I)	22.0 (1.4)
Refinement Statistics	
R_{work} (%) [2]	0.0981
R_{free} (%) [2]	0.1312
No. protein atoms	2600
No. water atoms	304
No. ligand atoms	194
Mean overall B value ($Å^2$)	15.020
Data Used In Refinement	
Resolution range (Å)	35.99 – 1.25
Completeness for tange	97.48
Number of reflections	75156
r.m.s deviations from ideal geometry	
Bond lengths (Å)	0.0224
Bond angles (°)	2.1375
Ramachadran analysis[3]	
No. in favoured regions (%)	316 (97.2)
No. in allowed regions (%)	9 (2.8)
Outliers	0 (0)

Table 2. CypA and CypD binding using Fluorescence Polarization.

Compound	CypA Ki (nM)	K133I CypD Ki (nM)
CsA	22.5 ± 4.3	1.4 ± 1.6
JW47	504.5 ± 9.2	298.0 ± 17.9
SmBz	236.2 ± 8.4	202.1 ± 14.1

Table 3. Plasma and brain levels of Jw47 in ABH mice following a single 10 mg/kg dose.

Time	Plasma		Brain	
	µg/mL	µM	µg/g	nM
2h	13.74 ± 3.84	10.1	0.018 ± 0.0019	13.2
4h	4.90 ± 0.85	3.60	0.017 ± 0.0016	12.5

Figure 1

A

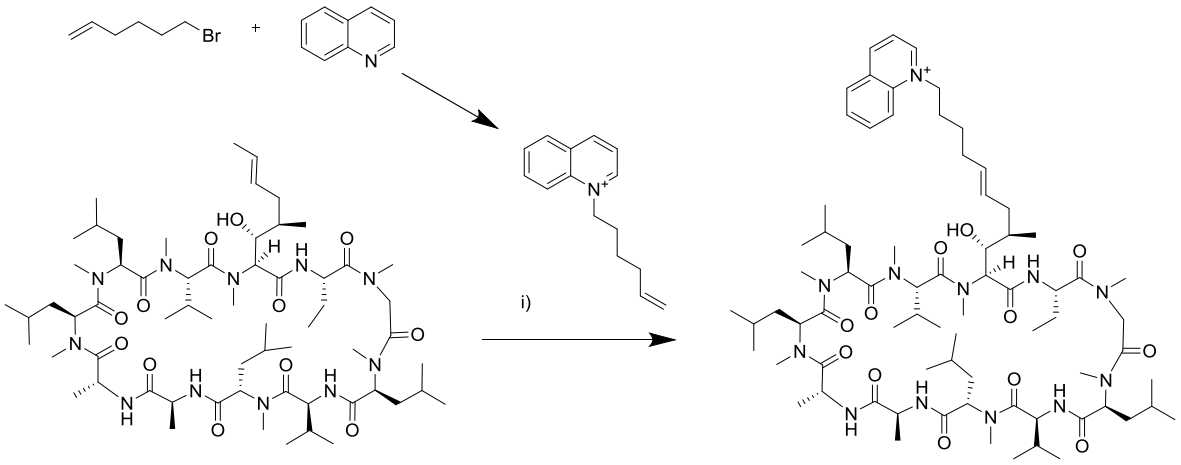

CsA JW47

B

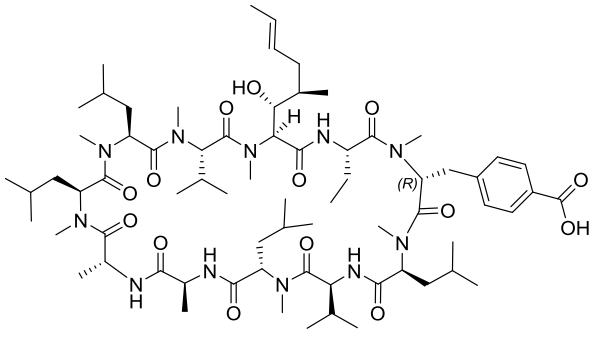

SmBzCsA

C

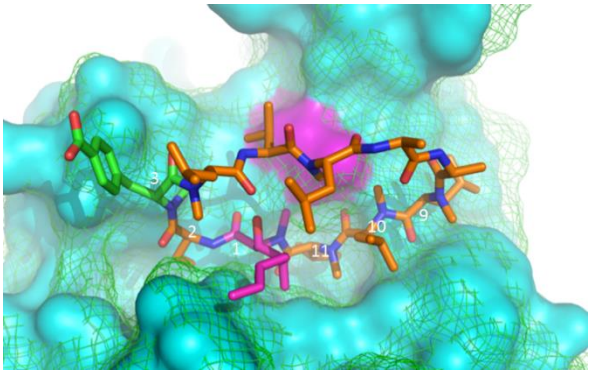

SmBzCsA crystal structure

Figure 2

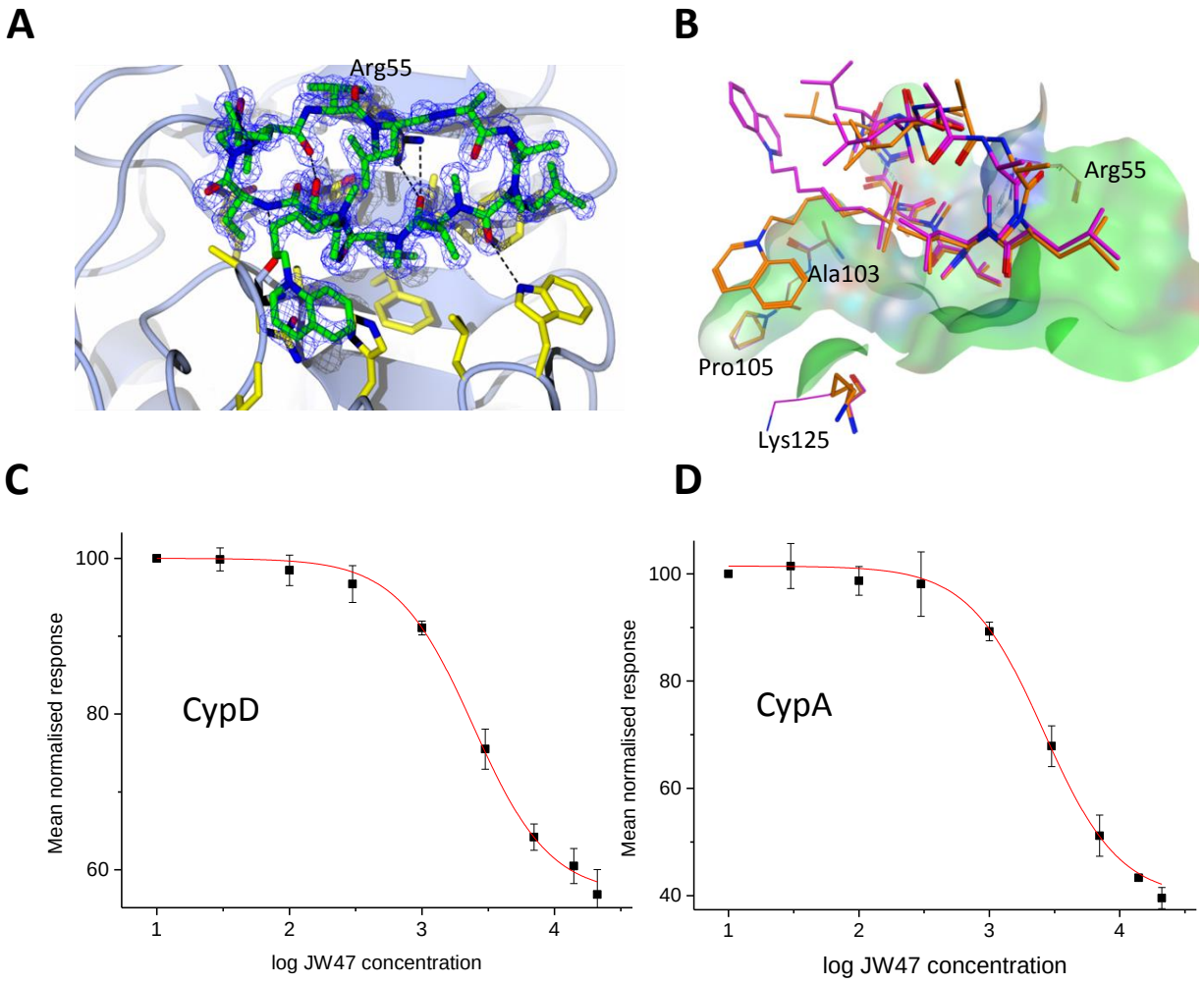
A
Arg55
B
Arg55
Ala103
Pro105
Lys125
C
CypD
Mean normalised response
log JW47 concentration
D
CypA
Mean normalised response
log JW47 concentration

Figure 3

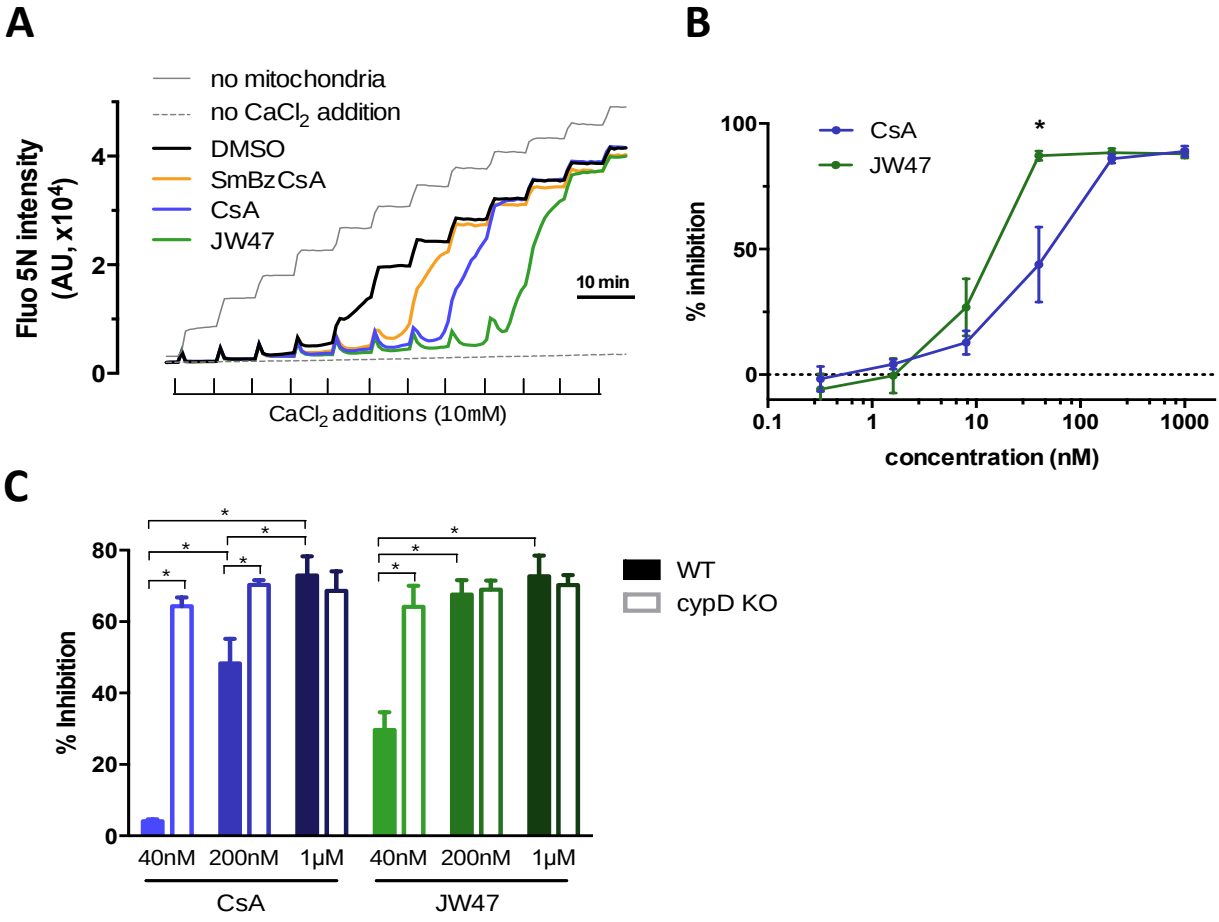
A
no mitochondria
no CaCl2 addition
DMSO
SmBzCsA
CsA
JW47
Fluo 5N intensity (AU, x10⁴)
10 min
CaCl2 additions (10mM)
B
CsA
JW47
*
% inhibition
concentration (nM)
C
% Inhibition
WT
cypD KO
40nM
200nM
1µM
40nM
200nM
1µM
CsA
JW47

Figure 4

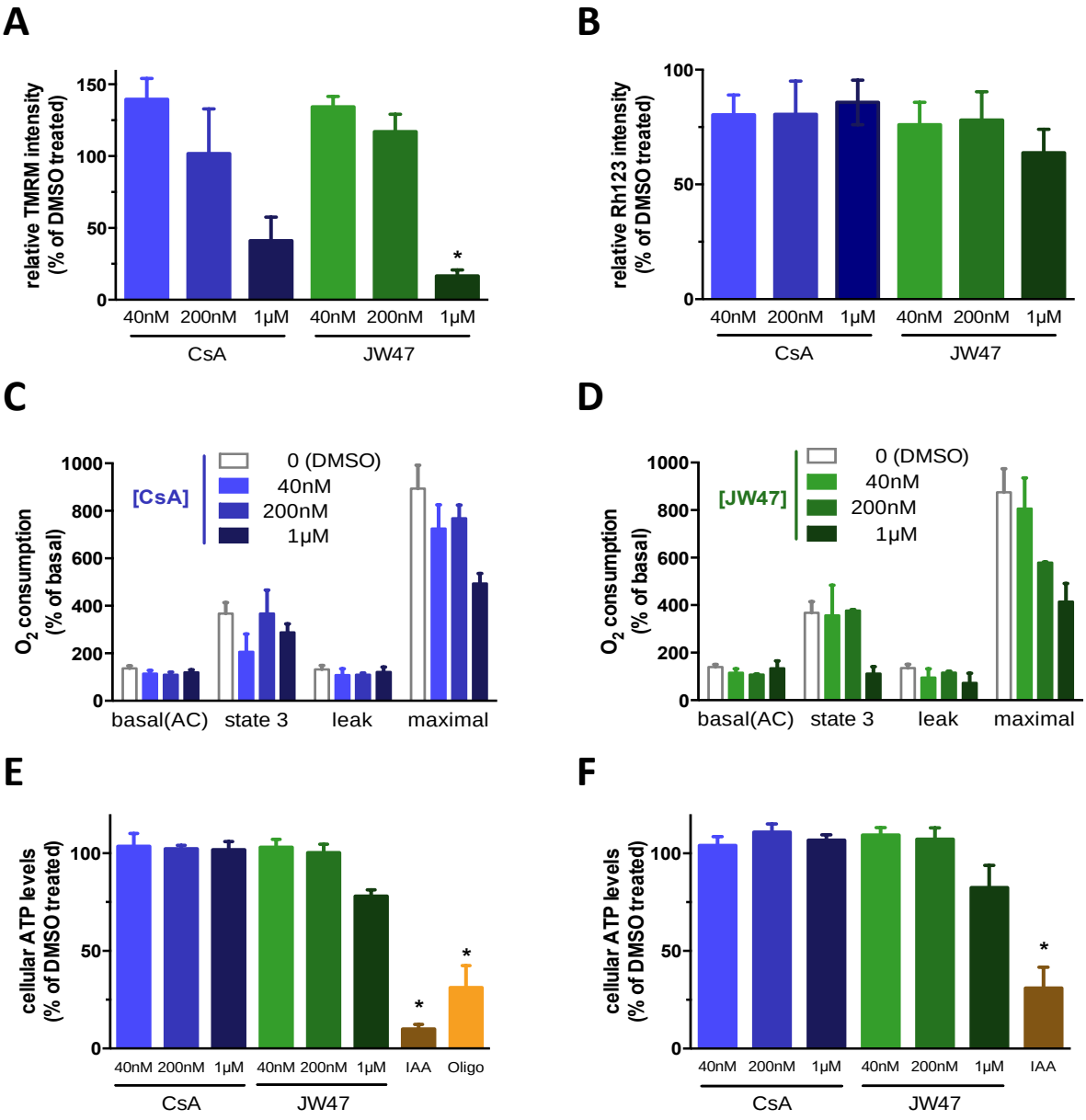
A
relative TMRM intensity (% of DMSO treated)
150
100
50
0
*
40nM 200nM 1µM 40nM 200nM 1µM
CsA
JW47
B
relative Rh123 intensity (% of DMSO treated)
100
50
0
40nM 200nM 1µM 40nM 200nM 1µM
CsA
JW47
C
O2 consumption (% of basal)
1000
800
600
400
200
0
[CsA]
0 (DMSO)
40nM
200nM
1µM
basal(AC) state 3 leak maximal
D
O2 consumption (% of basal)
1000
800
600
400
200
0
[JW47]
0 (DMSO)
40nM
200nM
1µM
basal(AC) state 3 leak maximal
E
cellular ATP levels (% of DMSO treated)
100
50
0
*
*
40nM 200nM 1µM 40nM 200nM 1µM IAA Oligo
CsA
JW47
F
cellular ATP levels (% of DMSO treated)
100
50
0
*
40nM 200nM 1µM 40nM 200nM 1µM IAA
CsA
JW47

Figure 5

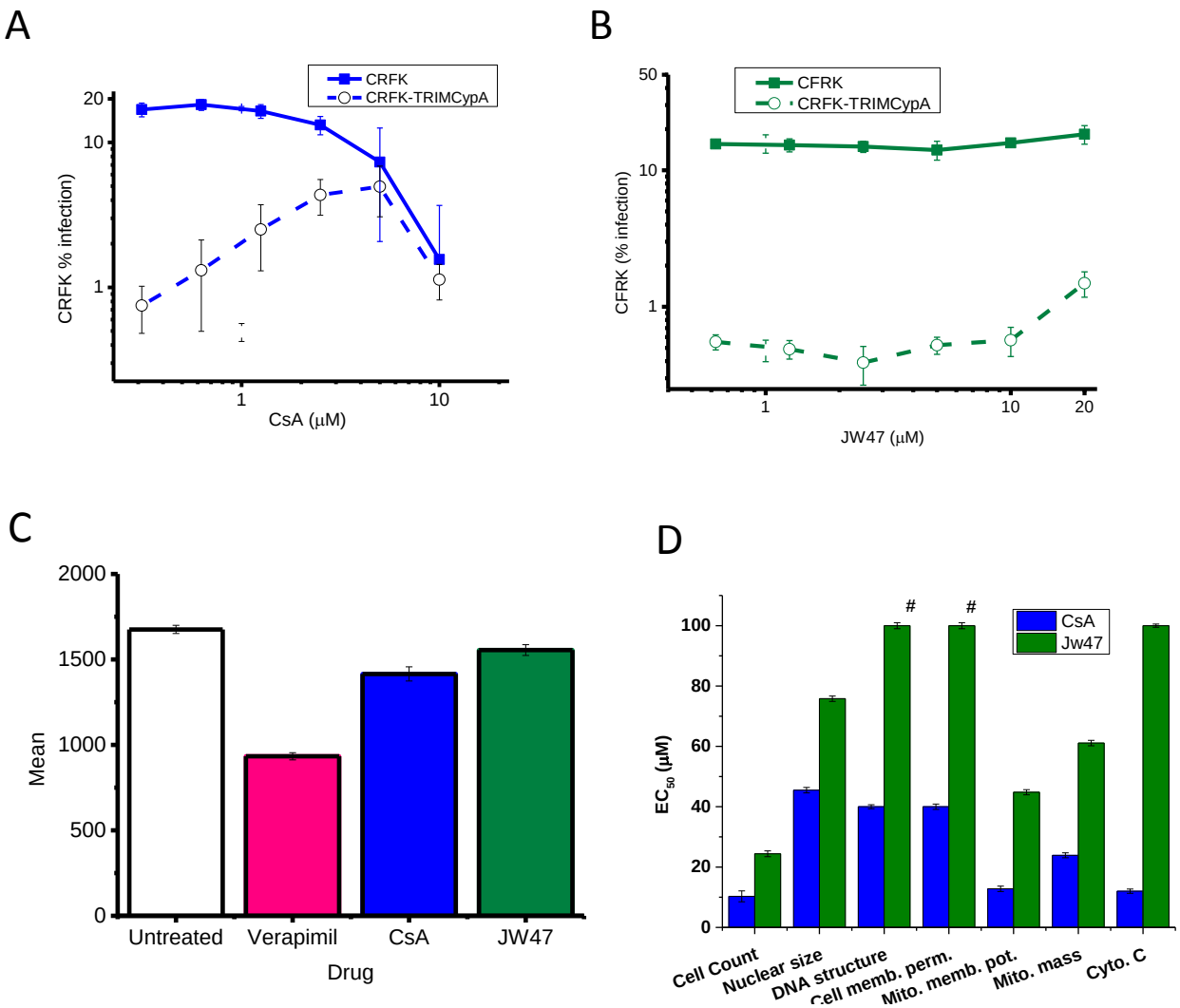
A
CRFK
CRFK-TRIMCypA
CRFK % infection)
20
10
1
1
10
CsA (μM)
B
CRFK
CRFK-TRIMCypA
CFRK (% infection)
50
10
1
1
10
20
JW47 (μM)
C
Mean
2000
1500
1000
500
0
Untreated
Verapimil
CsA
JW47
Drug
D
CsA
Jw47
EC50 (μM)
100
80
60
40
20
0
#
#
Cell Count
Nuclear size
DNA structure
cell memb. perm.
Mito. memb. pot.
Mito. mass
Cyto. C

Figure 6

A

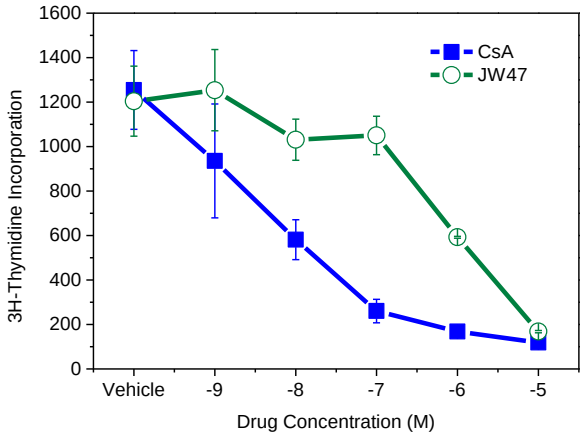

B

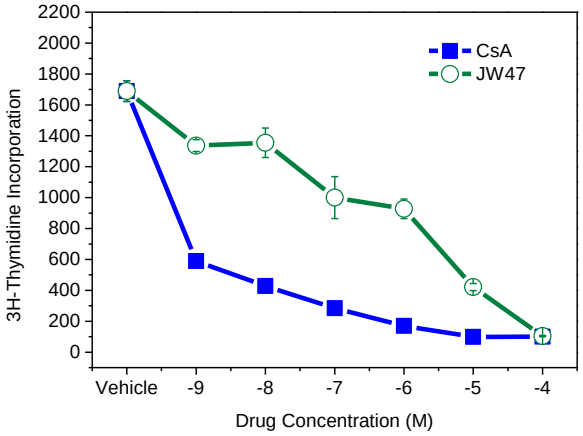

C

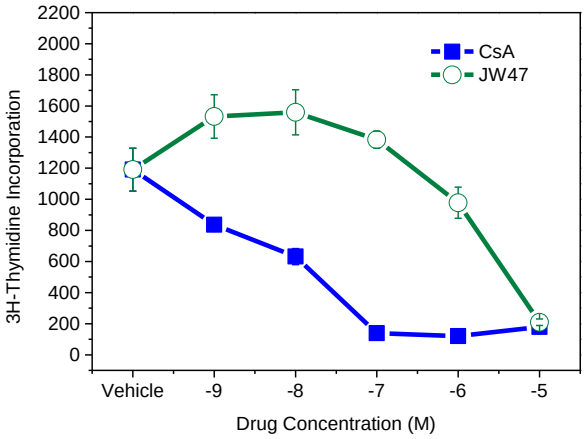

D

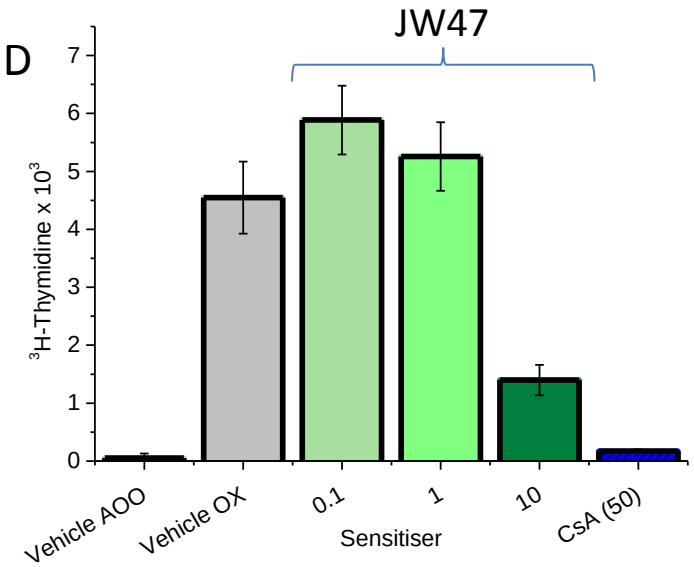

Figure 7

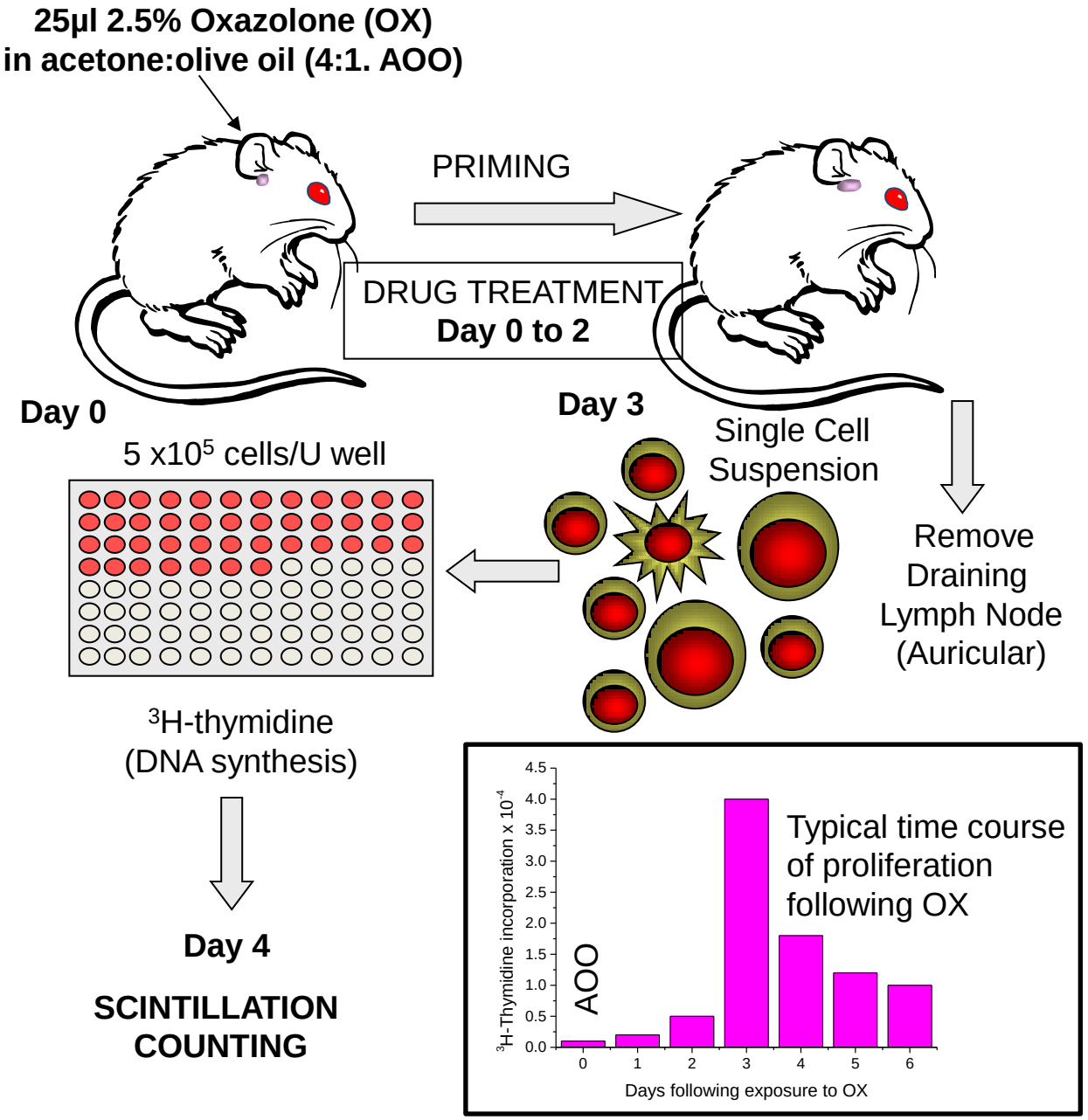
25µl 2.5% Oxazolone (OX)
in acetone:olive oil (4:1. AOO)
PRIMING
DRUG TREATMENT
Day 0 to 2
Day 0
Day 3
5 x10^5 cells/U well
Single Cell
Suspension
Remove
Draining
Lymph Node
(Auricular)
^{3}H-thymidine
(DNA synthesis)
Day 4
SCINTILLATION
COUNTING
AOO
^{3}H-Thymidine incorporation x 10^{-4}
Days following exposure to OX
Typical time course
of proliferation
following OX

Figure 8

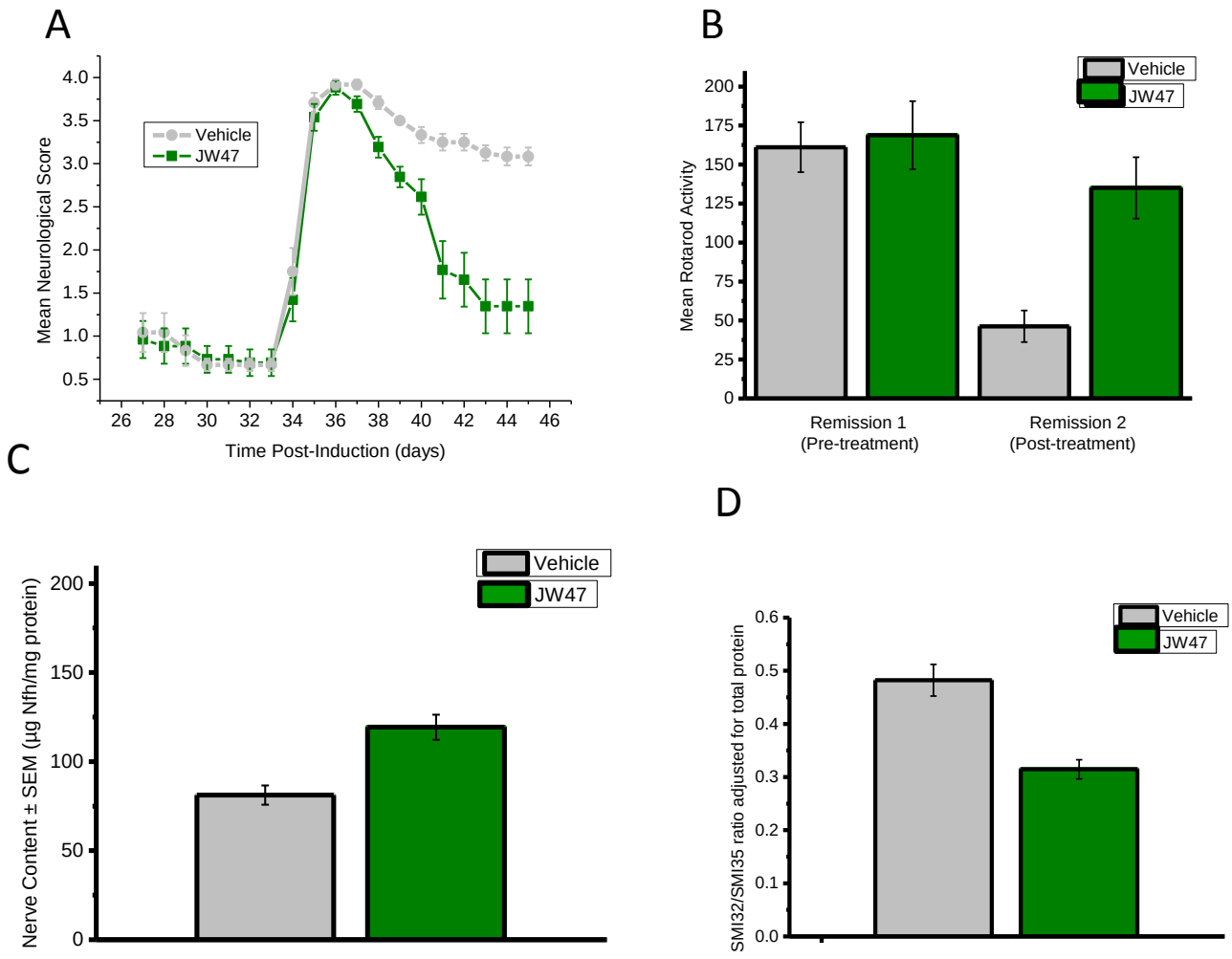
A
Mean Neurological Score
Time Post-Induction (days)
Vehicle
JW47
B
Mean Rotarod Activity
Remission 1
(Pre-treatment)
Remission 2
(Post-treatment)
Vehicle
JW47
C
Nerve Content ± SEM (µg Nfh/mg protein)
Vehicle
JW47
D
SMI32/SMI35 ratio adjusted for total protein
Vehicle
JW47

Supplementary methods

Selective inhibition of the mitochondrial permeability transition pore protects against neuro-degeneration in EAE multiple sclerosis.

Justin Warne, Gareth Pryce, Julia Hill, Xiao Shi, Felicia Lennerås, Fabiola Puentes, Maarten Kip, Laura Hilditch, Paul Walker, Michela I. Simone, A.W. Edith Chan, Greg J. Towers, Alun Coker, Michael R Duchen, Gyorgy Szabadkai, David Baker*, David L Selwood*.

Contents

Chemistry

All commercially available solvents and reagents were used without further treatment as received unless otherwise noted. NMR spectra were measured with a Bruker DRX 500 or 600 MHz spectrometer; chemical shifts are expressed in ppm relative to TMS as an internal standard and coupling constants (J) in Hz. LC-MS spectra were obtained using a Waters ZQ2000 single quadrupole mass spectrometer with electrospray ionisation (ESI), using an analytical C4 column (Phenomenex Gemini, 50 x 3.6 mm, 5 μm) and an AB gradient of 50–95 % for B at a flow rate of 1 mL/minute, where eluent A was 0.1:5:95 formic acid/methanol/water and eluent B was 0.:5:95 formic acid/water/methanol. High resolution mass spectra were acquired on a Waters LCT time of flight mass spectrometer with electrospray ionisation (ESI) or chemical ionization (CI).

Preparation of the fluorescein labelled cyclosporine (FP-CsA).

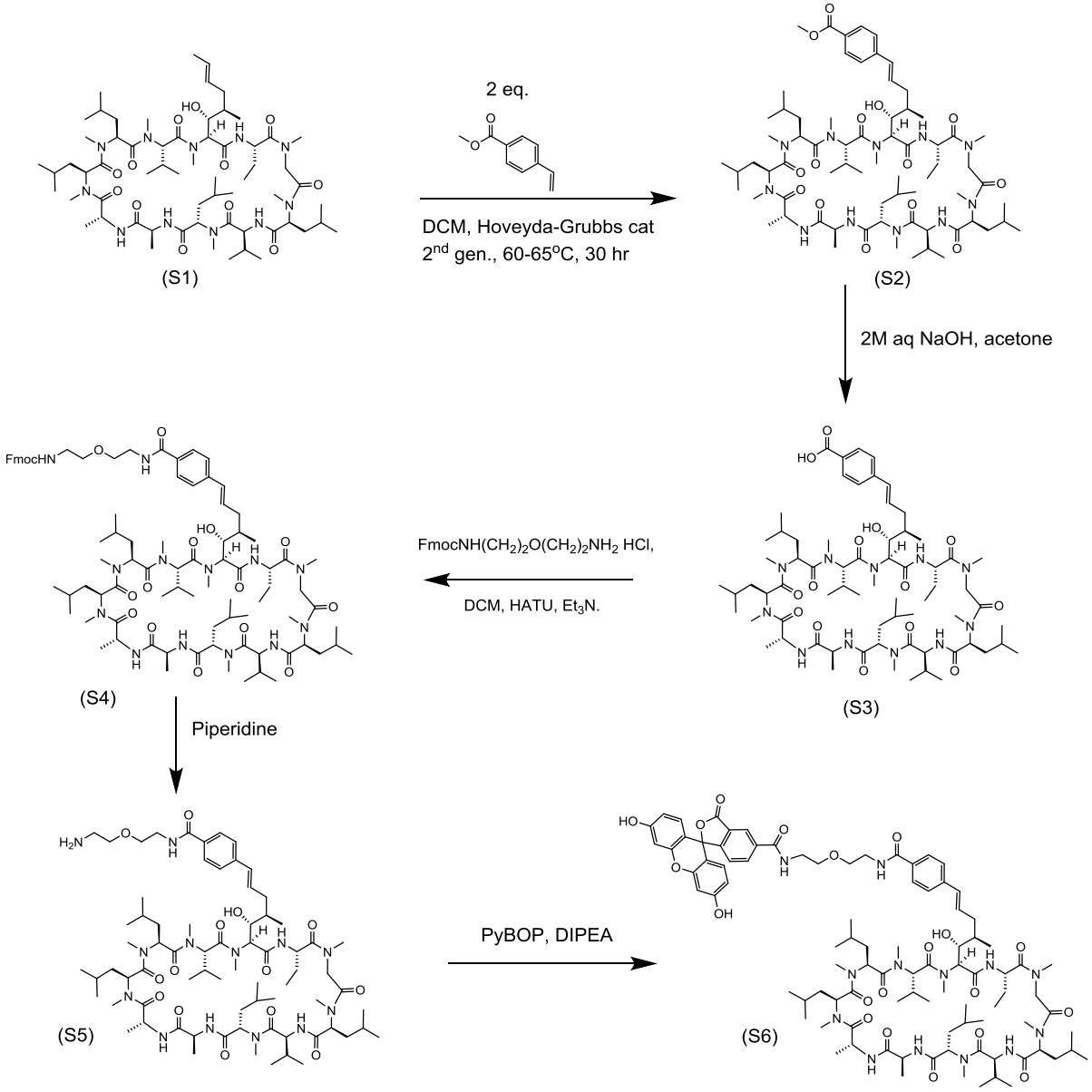

Formation of the vinyl methyl ester derivative (S2) from cyclosporine (S1).

A solution of cyclosporine (1.00 g, 0.832 mmol), methyl-4-vinylbenzoate (270 mg, 1.665 mmol) and Hoveyda-Grubbs 2nd generation catalyst (20 mg, 0.032, 4%) in dichloromethane (4 ml) was stirred at reflux (60°C) under nitrogen for 48 hours. T.l.c. analysis (acetone : cyclohexane, 1:1) of the reaction mixture showed the presence of the product (R_f 0.63) and complete consumption of the cyclosporine A starting material (R_f 0.65). LCMS analysis also confirmed the presence of the product. The reaction mixture was pre-absorbed on silica gel and purified by flash column chromatography (ethyl acetate : cyclohexane, 1:1 to ethyl acetate to ethyl acetate : methanol, 10%) and the solvent removed *in vacuo* to give a grey solid. The grey solid was then further purified by removing the Grubbs-Hoveida catalyst by letting it through an SPE-thiol column (eluant: methanol). The solvent was removed *in vacuo* to give the corresponding methyl ester as a white crystalline solid (950 mg, 86.4%).

HRMS (TOF MS ES$^+$): found 1344.8726 $[M+Na]^+$ $C_{69}H_{115}N_{11}O_{14}Na$ requires 1344.8523;

ν_{max} (thin film, KBr): 3466, 3418, 3318 (m-s, bumpy, CON-Hs, OH), 2961, 2935, 2873 (m, alkyl C-H), 1720 (m, conjugated C=OOMe), 1627 (s broad, bumpy, C=Os, amide I), 1520 (m broad, bumpy, C=Os, amide II) cm^{-1};

NMR δ_H ($CDCl_3$, 500 MHz): 7.92 (1H, d, J = 10.5 Hz, NH), 7.90 (2H, d, $J_{ArCH,ArCH}$ = 8.5 Hz, 2 x ArHs), 7.64 (1H, d, J = 8.0 Hz, NH), 7.47 (1H, d, J = 8.0 Hz, NH), 7.32 (2H, d, $J_{ArCH,ArCH}$ = 8.5 Hz, 2 x ArHs), 7.06 (1H, d, J = 7.5 Hz, NH), 6.34–6.24 (2H, m, alkene Hs), 5.62 (1H, dd, J = 10.5, 4.5 Hz, CαH), 5.48 (1H, d, J = 5.5 Hz, CαH, residue 1), 5.32-5.22 (2H, m, 2 x CαH), 5.07 (1H, d, J = 11.0 Hz, CαH, residue 11), 5.04-4.93 (2H, m, NHCα*H* + CαH), 4.90 (1H, dd, J = 10.0, 6.0 Hz, CαH), 4.77 (1H, app-q, J = 7.5 Hz, NHCα*H*), 4.69 (1H, d, J = 14.0 Hz, residue 3, CαH^{Re}*H*^{Si}), 4.60 (1H, app-t, J = 9.0 Hz, NHCα*H*), 4.47 (1H, app-q, J = 7.5 Hz, NHCα*H*), 4.50-4.37 (1H, m, Cα*H*), 4.26-4.10 (1H, broad s, OH), 3.84 (3H, s, CO_2Me), 3.76 (1H, app-t, J = 7.0 Hz, Cβ*H*-OH, residue 1), 3.48, 3.33, 3.23 (9H, 3 x s, 3 x N-Me), 3.19-3.15 (1H, m, residue 3, Cα*H*^{Re}H^{Si}), 3.05, 3.04 (6H, 2 x s, 2 x N-Me), 2.70-2.65 (1H, m, obscured, Ar-CH=CH-C*H*^{A}H^B), 2.66, 2.62 (6H, 2 x s, 2 x N-Me), 1.87-1.80 (1H, m, Ar-CH=CH-CH^A*H*^{B}), 2.42-2.30, 2.10-0.60 (side-chain alkyl Hs, all residues);

NMR δ_C ($CDCl_3$, 125 MHz): 173.84 (C=O), 173.81(C=O), 173.74 (C=O), 173.50 (C=O), 171.54 (C=O), 171.17 (C=O), 170.50 (C=O), 170.44 (2 x C=O), 170.26 (C=O), 170.18 (C=O), 167.06 (C=O ester), 142.44 (Ar*C*q-CH=CH), 132.85 (ArCq-*C*H=CH), 130.63 (ArCq-CH=*C*H), 129.88, 125.91 (2 x 2Cs, 4 x ArCs), 128.19 (*C*q-COOMe), 75.05 (CαH-*C*H[side chain]-OH, residue 1), 58.74, 57.97, 57.56, 55.53 (2 Cs), 55.38 (6 x CαH), 51.98 (OMe ester), 50.40 (CαH_2, residue 3), 48.85, 48.58, 48.26, 45.18 (4 x CαH), 40.50, 38.98, 37.50, 36.38, 36.02 (5Cs, 4 x CαH-*C*H_2-CH$(CH_3)_2$, residues 4, 6, 9 and 10; (CαH-CH[OH]-*C*H[side chain]-CH_3), residue 1), 39.46 (N-Me), 36.77 (ArCq-CH=CH-*C*H_2, residue 1), 34.13 (N-Me), 31.58 (N-Me), 31.36 (N-Me), 31.12 (N-Me), 29.81 (N-Me), 29.60 (N-Me), 29.84, 29.30, 29.14, 25.36, 24.99, 24.90, 24.66, 24.40, 23.81, 23.71, 23.40, 21.92, 21.83, 21.27, 20.37, 19.87 (15 Cs, 4 x CH(*C*$H_3)_2$ and 4 x *C*H$(CH_3)_2$, residues 4, 6, 9 and 10; 2 x *C*H$(CH_3)_2$, residues 5 and 11; CαH-*C*H_2-CH_3, residue 2), 18.72, 18.45 (2 x 2Cs, 4Cs, 2 x valine [CH(*C*$H_3)_2$]), 18.20, 16.90 (2Cs, 2 x CαH-*C*H_3, residues 7 and 8), 16.10 (CαH-CH[OH]-CH[side chain]-*C*H_3, residue 1), 9.93 (CαH-CH_2-*C*H_3, residue 2).

Formation of the Vinyl acid derivative (S3)

The methyl ester **S2** (260 mg, 0.196 mMol) was stirred in acetone (4 mL) and an aqueous solution of sodium hydroxide (2M, 2 mL). After 19 hours a white precipitate had formed and T.l.c. analysis (acetone : cyclohexane, 1: 1) showed the presence of one product (R_f 0.17) and some residual starting material/impurity (R_f 0.31). The acetone was removed from the reaction mixture and the aqueous layer left behind was washed with ethyl acetate. The aqueous layer was acidified with an aqueous solution of hydrochloric acid (1M) and washed again with ethyl acetate. The collected ethyl acetate layers were dried (magnesium sulfate), filtered and concentrated in vacuo to give a white/pale brown hygroscopic solid which was then diluted in acetonitrile and filtered again (eluant acetonitrile). The filtrate was finally concentrated in vacuo to give the acid derivative **3** (220 mg, 86%) as a white/pale brown hygroscopic solid.

HRMS (TOF MS ES$^+$): found 1330.8366 $[M+Na]^+$ $C_{68}H_{113}N_{11}O_{14}Na$ requires 1330.8173.

ν_{max} (thin film, KBr): 3418, 3315 (m, bumpy, CON-Hs, OH), 2961, 2936, 2873 (m, alkyl C-H), 1714 (m, conjugated C=OOH), 1627 (s broad, bumpy, C=Os, amide I), 1520 (m broad, bumpy, C=Os, amide II) cm^{-1}

NMR δ_H ($CDCl_3$, 500 MHz): (500 MHz, CDCl3) δ 3.51 (s, NMe, 3H), 3.37 (s, NMe, 3H), 3.23 (s, NMe, 3H), 3.09 (s, NMe, 3H), 3.08 (s, NMe, 3H), 2.68 (s, NMe, 3H), 2.65 (s, NMe, 3H).

NMR δ_C ($CDCl_3$, 125 MHz): 39.53, 34.19, 31.64, 31.35, 29.88 (2Cs), 29.61 (7 x N-Me).

Synthesis of Fmoc protected intermediate (S4)

HATU coupling reagent (230 mg, 0.6037 mMol) was added to a solution of the CsA acid **S3** derivative (395 mg, 0.3018 mMol), chloroform (10 mL) and triethylamine (168 µL) which had been stirring for 5 minutes under an atmosphere of nitrogen at room temperature. After a further 5 minutes 2-[2-(Fmoc-amino)ethoxy ethylamine hydrochloride (257 mg, 0.7083 mMol) was added to the stirring reaction mixture and left to react for 22.5 hours. LCMS analysis revealed the presence of the product in the reaction mixture. The reaction mixture was concentrated in vacuo and successively diluted in ethyl acetate and washed with an aq hydrochloric acid solution (1M). The collected organic layers were dried over magnesium sulphate, filtered and concentratedin vacuo to give a residue which was purified by flash column chromatography (chloroform to chloroform-methanol, 3%) to give the Fmoc derivative **S4** (406 mg, 83%) as a white hygroscopic solid.

HRMS (TOF MS ES^+): found 1638.9775 $[M+Na]^+$ $C_{87}H_{133}N_{13}O_{16}Na$ requires 1638.9891.

δ_H ($CDCl_3$, 500 MHz): 3.49 (s, NMe, 3H), 3.45 (s, NMe, 3H), 3.34 (s, NMe, 3H), 3.20 (s, NMe, 3H), 3.06 (s, NMe, 3H), 2.65 (s, NMe, 3H), 2.64 (s, NMe, 3H).

δ_C ($CDCl_3$, 125 MHz): 38.98, 33.97, 33.85, 31.77, 29.81 (2Cs), 29.66 (7 x N-Me).

Synthesis of the cyclosporin – PEG- amine derivative (S5).

To the FmoC protected CsA analogue **S4** (97 mg, 0.06 mMol) was added piperidine (0.5 mL), and the reaction was stirred overnight at rt. The piperidine was removed on a rotary evaporator and the residue purified by chromatography using 5-10% MeOH containing 2% 880 ammonia in CH_2Cl_2. This gave the intermediate amine **S5** (26 mg, 0.019 mMol, 31%) as yellow gum. This was used directly in the next step.

Synthesis of the fluorescein –PEG- CsA derivative (S6).

To the amine **S5** (22 mg, 18.6 mMol), 5/6-carboxyfluorescein (7 mg, 0.0187 mMol) and PyBOP (10 mg, 19 mMol) in CH_2Cl_2 (1 mL) was added diisopropylethylamine (9 mg, 13 µL, 76 mMol) and the reaction stirred overnight. The volatiles were removed on the rotary evaporator and the residue purified using reverse phase chromatography, C18, 5% MeOH to 95% MeOH in water. This gave the product **S6** (10 mg, 0.0057 mMol, 48%).

LCMS (ES+) 1775 ($M+Na^+$), 1752 ($M+H^+$). C18 >95%.

1-(10-Bromodecyl)quinolin-1-ium

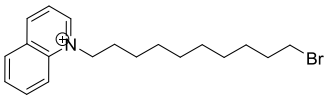

To a solution of quinoline (0.5 g, 3.87 mmol) in toluene was added 1,10-dibromodecane (1.74 g, 5.81 mmol) and this mixture was heated to 80°C for 48hrs. The mixture was allowed to cool before filtration. The solid was purified by column chromatography, eluting with 0-10% MeOH in DCM. The product was isolated as a clear oil (1.26 g, 93%).

^{1}H NMR (600 MHz, MeOD) δ 9.41 (dd, *J* = 5.8, 1.4 Hz, 1H), 9.21 (d, *J* = 8.3 Hz, 1H), 8.56 (d, *J* = 9.0 Hz, 1H), 8.44 (dd, *J* = 8.2, 1.4 Hz, 1H), 8.31 (ddd, *J* = 8.8, 7.0, 1.5 Hz, 1H), 8.15 – 8.01 (m, 2H), 5.09 (t, 2H), 3.43 (t, *J* = 6.7 Hz, 1H), 2.17 – 2.03 (m, 2H), 1.88 – 1.75 (m, 2H), 1.56 – 1.25 (m, 10H).

1-(10-((3-carboxy-4-(6-hydroxy-3-oxo-3H-xanthen-9-yl)benzoyl)oxy)decyl)quinolin-1-ium

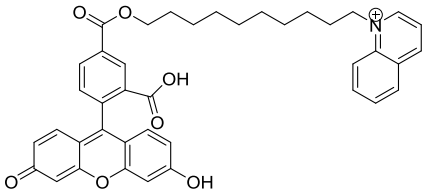

To a solution of 5-carboxyfluoroscein (0.065 g, 0.172 mmol) and sodium carbonate (0.04 g) in DMF was added dropwise a solution of 1-(10-bromodecyl)quinolinium (0.06 g, 0.172 mmol) in minimal DCM. This mixture was heated to 60°C overnight and was allowed to cool before dilution with DCM and washing with 1M citric acid. The organics were dried over $MgSO_4$ and concentrated under reduced pressure. The resultant orange solid was purified by column chromatography, eluting with 0-10% MeOH in DCM.

The product was isolated as a dark yellow solid (0.082 g, 75%).

^{1}H NMR (600 MHz, MeOD) δ 9.41 (d, *J* = 5.3 Hz, 1H), 9.16 (d, *J* = 8.3 Hz, 1H), 8.56 – 8.50 (m, 2H), 8.40 (d, *J* = 8.1 Hz, 1H), 8.35 (dd, *J* = 8.0, 1.3 Hz, 1H), 8.28 – 8.22 (m, 1H), 8.05 (dd, *J* = 8.3, 5.8 Hz, 1H), 8.01 (t, *J* = 7.6 Hz, 1H), 7.31 (d, *J* = 8.0 Hz, 1H), 6.67 (t, *J* = 3.5 Hz, 2H), 6.55 (d, *J* = 8.7 Hz, 2H), 6.53 – 6.48 (m, 2H), 5.13 – 5.00 (m, 2H), 4.38 (t, *J* = 6.4 Hz, 2H), 2.19 – 2.01 (m, 2H), 1.92 – 1.73 (m, 2H), 1.52 – 1.32 (m, 12H).

Selective inhibition of the mitochondrial permeability transition pore protects against neuro-degeneration in experimental multiple sclerosis.

Justin Warne, Gareth Pryce, Julia Hill, Xiao Shi, Felicia Lennerås, Fabiola Puentes, Maarten Kip, Laura Hilditch, Paul Walker, Michela I. Simone, A.W. Edith Chan, Greg J. Towers, Alun Coker, Michael R. Duchen, Gyorgy Szabadkai, David Baker and David L. Selwood

J. Biol. Chem. published online December 17, 2015
